2017

Sequences within the C terminus of the metabotropic glutamate receptor 5 (mGluR5) are responsible for inner nuclear membrane localization

Ismail Sergin
Washington University School of Medicine in St. Louis

Yuh-Jiin I. Jong
Washington University School of Medicine in St. Louis

Steven K. Harmon
Washington University School of Medicine in St. Louis

Vikas Kumar
Washington University School of Medicine in St. Louis

Karen L. O'Malley
Washington University School of Medicine in St. Louis

THE JOURNAL OF BIOLOGICAL CHEMISTRY VOL. 292, NO. 9, pp. 3637–3655, March 3, 2017

Sequences within the C Terminus of the Metabotropic Glutamate Receptor 5 (mGluR5) Are Responsible for Inner Nuclear Membrane Localization*

Received for publication, September 8, 2016, and in revised form, January 12, 2017 Published, JBC Papers in Press, January 17, 2017, DOI 10.1074/jbc.M116.757724

Ismail Sergin[1], **Yuh-Jiin I. Jong**[1], **Steven K. Harmon, Vikas Kumar, and Karen L. O'Malley**[2]

From the Department of Neuroscience, Washington University School of Medicine, St. Louis, Missouri 63110

Edited by Roger J. Colbran

Traditionally, G-protein-coupled receptors (GPCR) are thought to be located on the cell surface where they transmit extracellular signals to the cytoplasm. However, recent studies indicate that some GPCRs are also localized to various subcellular compartments such as the nucleus where they appear required for various biological functions. For example, the metabotropic glutamate receptor 5 (mGluR5) is concentrated at the inner nuclear membrane (INM) where it mediates Ca^{2+} changes in the nucleoplasm by coupling with $G_{q/11}$. Here, we identified a region within the C-terminal domain (amino acids 852–876) that is necessary and sufficient for INM localization of the receptor. Because these sequences do not correspond to known nuclear localization signal motifs, they represent a new motif for INM trafficking. mGluR5 is also trafficked to the plasma membrane where it undergoes re-cycling/degradation in a separate receptor pool, one that does not interact with the nuclear mGluR5 pool. Finally, our data suggest that once at the INM, mGluR5 is stably retained via interactions with chromatin. Thus, mGluR5 is perfectly positioned to regulate nucleoplasmic Ca^{2+} *in situ*.

From their position on the cell surface, G-protein-coupled receptors (GPCRs)[3] can transform external stimuli into a broad range of signaling pathways within the cell. A mounting body of evidence indicates that many GPCRs are also localized inside the cell where they may couple to different signaling systems, display unique desensitization patterns, and/or exhibit distinct patterns of subcellular distribution (1–5). For example, GPCRs have been found on mitochondria (6), endoplasmic reticulum (ER) membranes (7), lysosomes (8, 9), and on nuclear membranes (10–12). Certain GPCRs are even found within the nucleoplasm on nuclear bodies and/or nuclear invaginations (13–16). Although many intracellular GPCRs are activated at the cell surface and subsequently trafficked to their intracellular site, others can be activated at their subcellular location via so-called intracrine ligands that can enter cells via diffusion or be made *in situ*, endocytosed, and/or transported through channels or pores (12, 17, 18). Intracellular GPCRs can also function independently governing processes such as synaptic plasticity (19), myocyte contraction (15), and angiogenesis (16). Collectively, the present findings reinforce the notion that intracellular GPCRs play a dynamic role in generating and shaping intracellular signaling pathways.

As many GPCRs are on or in the nucleus, the question arises as to how they get there. Various possibilities exist to transfer membrane proteins from the outer to the inner nuclear membrane (ONM and INM), including vesicle fusion, membrane rupture, and channel-mediated pathways. Most prominently, a diffusion-retention model has been proposed for many INM proteins (*e.g.* lamin B receptor (*LBR*)) (20, 21). This model suggests that proteins synthesized in the ER rapidly diffuse laterally in the ONM, pass through peripheral channels existing between the nuclear pore complex and the pore membrane, and then become tethered in the INM via nucleoplasmic interactions with nuclear lamins or chromatin (22–24). Because the peripheral channels are thought to be about 10 nm, nucleoplasmic domains cannot exceed masses of >60 kDa (25–27). Although the exact signals are unknown, at least 15 proteins have been shown to translocate through peripheral channels to reside on the INM (20, 21, 28). Current findings show that a wide range of mechanisms underlie transmembrane INM transport, including use of phenylalanine-glycine (FG) motifs, use of nucleoporins, and use of the peripheral channels or the central channel or both (20, 21). Certain INM proteins also contain an NLS, although mutation or deletion does not affect INM localization (20). Many peptide-activated GPCRs also use an NLS and karyopherins such as importin-β1 for nuclear import after receptor activation on the cell surface (16). Inasmuch as these receptors are not associated with the INM but rather appear within the nucleoplasm itself (via unknown

* This work was supported, in whole or in part, by National Institutes of Health Grants MH109019, MH57817, and MH69646 (to K. L. O.), and the Simons Foundation Grant NS081454. The authors declare that they have no conflicts of interest with the contents of this article. The content is solely the responsibility of the authors and does not necessarily represent the official views of the National Institutes of Health.

[1] Both authors contributed equally to this work.

[2] To whom correspondence should be addressed: 660 S. Euclid Ave., Campus Box 8108, St. Louis, MO 63110. Tel.: 314-362-7087; Fax: 314-362-3446; E-mail: omalleyk@wustl.edu.

[3] The abbreviations used are: GPCR, G-protein-coupled receptor; INM, inner nuclear membrane; ER, endoplasmic reticulum; NES, nuclear exclusion signal; NLS, nuclear localization signal; IP_3, inositol 1,4,5-trisphosphate; ONM, outer nuclear membrane; LBR, lamin B receptor; PM, plasma membrane; NM, nuclear membrane; Endo H, endo-β-*N*-acetylglucosaminidase H; ROI, region of interest; DHPG, (*S*)-3,5-dihydroxyphenylglycine; PNGase, peptide:*N*-glycosidase; MPEP, 2-methyl-6-(phenylethynyl) pyridine; mGluR5, metabotropic glutamate receptor 5; Quis, L-quisqualic acid LY53, LY393053; BBS, bungarotoxin-binding site; BAPTA AM, 1,2-bis(2-aminophenoxy)ethane-*N*,*N*,*N*′,*N*′-tetraacetic acid tetrakis(acetoxymethyl ester); FRAP, fluorescence recovery after photobleaching; RFP, red fluorescent protein.

mechanisms), the nucleoplasm targeting motifs might be quite different. Thus, unlike karyopherin-mediated transport of soluble proteins, targeting proteins to the INM is more varied and complex.

One intracellular GPCR found on the INM is the metabotropic glutamate receptor 5 (mGluR5). mGluR5 plays a key role in normal neurodevelopment as well as in many neurodevelopmental and neurological disorders such as Fragile X syndrome/Autism Spectrum Disorders, anxiety, schizophrenia, drug addiction, Parkinson's disease, dyskinesias, and chronic pain (1). Although mGluR5 is found on the plasma membrane, 60–90% of the receptor is associated with intracellular membranes like the INM (29–33). Pharmacological isolation and genetic manipulation have allowed us to determine that INM mGluR5 couples to $G_{q/11}$ leading to a large sustained release of luminal Ca^{2+}, phosphorylation of nuclear *Erk1/2*, and activation of immediate early genes such as *Elk-1*, *Fos*, *Fosl1*, and *FosL2*, and immediate early effector proteins such as *Arc* (34–36). Physiologically, intracellular mGluR5 contributes to long term depression in the hippocampus (19) and pathological pain in the spinal cord dorsal horn (33). To further dissect mGluR5's subcellular functions, defining the sequence motifs responsible for its localization is necessary. Using molecular, immunological, and optical techniques, here we show that 25 amino acids within the mGluR5 nucleoplasmic domain are necessary and sufficient for its localization to the INM. Moreover, mGluR5 appears to be tethered in place via interactions with chromatin. Thus, mGluR5 appears to use a non-canonical signal sequence-retention strategy to anchor itself on the INM where it is poised to regulate transcription (35), chromosome remodeling, and genomic integrity.

Results

mGluR5 C Terminus Is Necessary and Sufficient for Nuclear Membrane Localization—Previously, we have shown that mGluR5 can be expressed on the PM and on intracellular membranes, including the ER, ONM, and INM (30, 31, 33). To date, no motifs responsible for maintaining mGluR5 or other INM GPCRs in this location have been described. Because trafficking of GPCRs is often dictated by sequences within the cytoplasmic tail (37–41), we hypothesized that the mGluR5 C terminus is the domain required for INM localization. To test this idea, we prepared HA-tagged chimeric constructs derived from mGluR5 and the closely related $GABA_{B2}$ GPCR. Typically, $GABA_{B2}$ receptors form heterodimers with $GABA_{B1}$, masking an ER retention signal (42), following which the heterodimer is efficiently transported to the PM (43). Because $GABA_{B2}$ always traffics to the PM, it serves as a control for PM localization. Thus, chimeric plasmids were created in which the C termini of mGluR5 and $GABA_{B2}$ were swapped (Fig. 1*A*).

For this experiment and others described below, HA-tagged control and chimeric receptors were transiently transfected into HEK293 cells and subsequently stained for PM expression using antibodies directed against HA on non-permeabilized cells. All constructs showed at least some level of PM expression, although absolute amounts varied as indicated by the line scans and western blots associated with Figs. 1 and 2 (and data not shown). Because the HA tag is in the extracellular ligand binding domain, these results suggest that introduced receptors assume the correct orientation within the PM and that regardless of the described manipulation, the receptor could be found on the PM.

Immunocytochemical analyses of permeabilized cells revealed that the chimeric receptor, $N_{mG5}C_{GB2}$, was found predominately at the cell surface whereas $N_{GB2}C_{mG5}$ was on NM and ER membranes. In particular, $N_{GB2}C_{mG5}$ co-localized with the NM marker lamin B_2 whereas $N_{mG5}C_{GB2}$ did not (Fig. 1*A*). Line scan analysis corroborated that mGluR5 and $N_{GB2}C_{mG5}$ co-localized with lamin B_2 on NM (Fig. 1, *A*–*C*). We also assessed the intensity of fluorescent signals detected on either the PM or NM across multiple experiments. These results confirmed that the C terminus of mGluR5 prevented the chimeric $N_{GB2}C_{mG5}$ from going to the cell surface, and in contrast, the $GABA_{B2}$ C terminus predominantly localized mGluR5 lacking its C terminus at the PM (Fig. 1, *A* and *D*). To confirm and extend these results, we used subcellular fractionation. Following transient transfection, mGluR5 was readily visible in NM fractions (Fig. 2*A*), whereas $GABA_{B2}$ was not (Fig. 2*B*). Consistent with the immunocytochemistry, the $N_{mG5}C_{GB2}$ construct was primarily detected in the PM fraction (Fig. 2*C*); whereas $N_{GB2}C_{mG5}$ was detected in both PM and nuclear fractions (Fig. 2*D*). Quantitation of results from multiple experiments is shown in Fig. 2*E*. Treatment with 1 mM glutamate or baclofen (mGluR5 and $GABA_{B2}$ agonists, respectively) did not produce an obvious re-distribution of receptor subtypes in these cultures (Fig. 11*B*, and not shown). Taken together, these data indicate that the C terminus is necessary and sufficient for NM localization of mGluR5.

mGluR5 C-terminal Amino Acids 852–876 Are Responsible for Nuclear Membrane Localization—To further define regions critical for NM localization, we prepared three different constructs to examine the involvement of the proximal regions of the mGluR5 C terminus for NM localization. Because the size of the C-terminal region available to go through the nuclear pore might influence its ability to do so (22), additional constructs were deliberately kept within the size range of the original mGluR5 C terminus. Thus, constructs were similar to the $N_{mG5}C_{GB2}$ construct but carried small C-terminal extensions downstream of the seventh transmembrane domain of mGluR5 before the addition of the $GABA_{B2}$ C terminus (Fig. 3*A*). Distribution and orientation of the constructs $N_{mG5\_854}C_{GB2}$, $N_{mG5\_896}C_{GB2}$, and $N_{mG5\_966}C_{GB2}$ were examined by immunostaining and subcellular fractionation methods (Fig. 3, *A*–*G*). Lamin B_2 co-localization was observed for the $N_{mG5\_896}C_{GB2}$ and $N_{mG5\_966}C_{GB2}$ constructs in HEK293 cells; however, $N_{mG5\_854}C_{GB2}$ was primarily localized on the PM (Fig. 3, *A*–*C*). This distribution pattern was further confirmed by subcellular fractionation (Fig. 3, *D*–*G*). Occasionally, doublet bands were seen in some PM and NM fractions, which presumably reflect the glycosylation state of the receptor at the time of processing. This interpretation is consistent with results below (Fig. 11*A*), in which similar doublets were seen prior to PNGase F treatment but not afterward. These results suggest that mGluR5 amino acids 855–896 are required for NM localization.

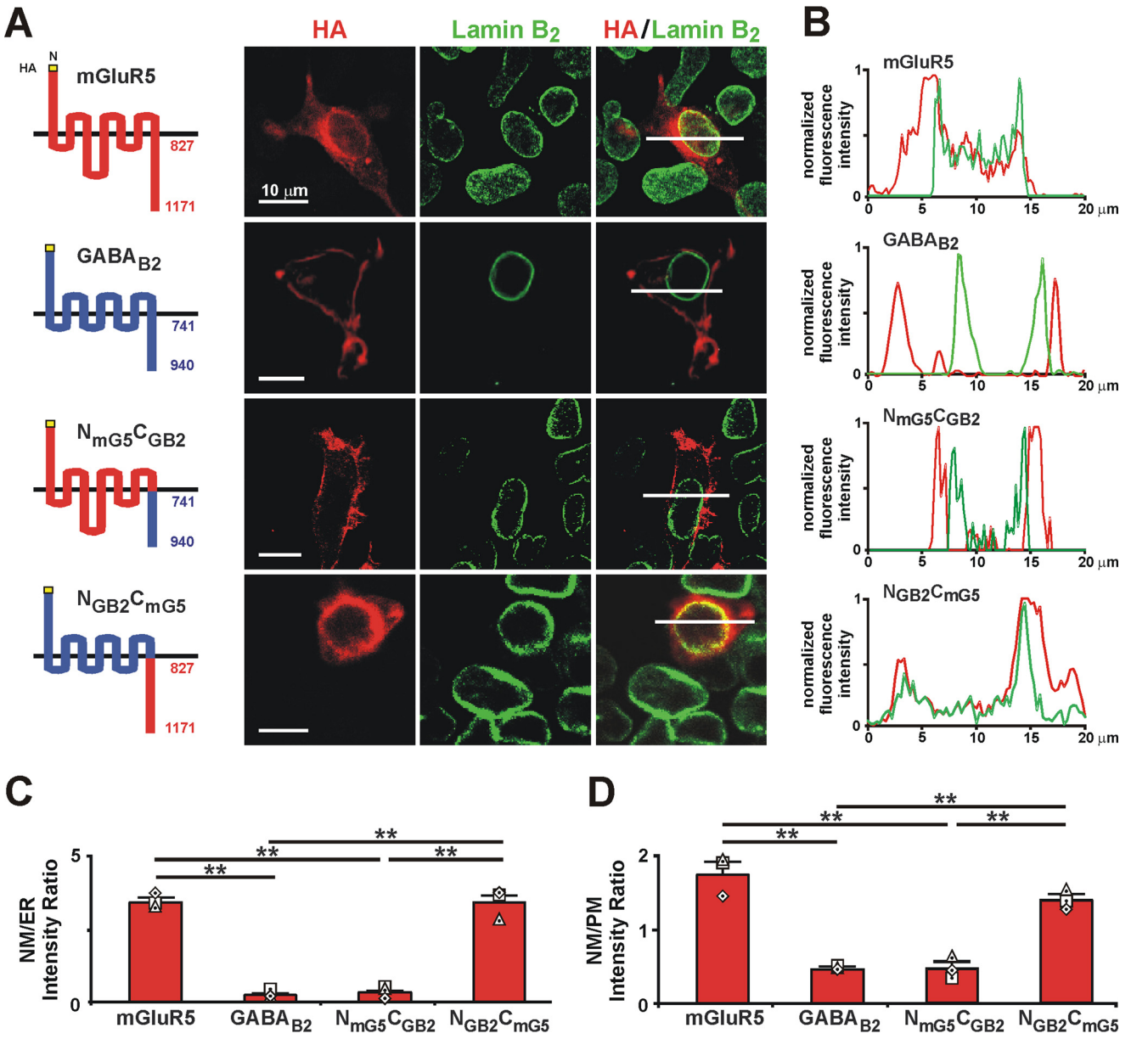

FIGURE 1. **Intracellular C terminus of mGluR5 is necessary and sufficient for nuclear membrane localization of the receptor.** *A,* co-localization of the full-length or chimeric constructs with NM marker lamin B_2. Schematic illustrations of the constructs that were transfected and tested for nuclear localization in HEK293 cells are next to each cellular pattern of expression. All constructs are HA-tagged at their N terminus. *Numbers* represent corresponding amino acid residues where the intracellular C terminus starts and the protein ends. *Yellow bars* indicate the HA tag; *red bars* indicate mGluR5; and *blue bars* indicate $GABA_{B2}$ receptor sequences. In chimeric constructs the mGluR5 C-terminal sequences are replaced by the $GABA_{B2}$ C terminus or vice versa. HEK293 cells were transfected with the constructs shown in *A,* fixed, and processed for immunohistochemistry using HA and lamin B_2 antibodies. Cells were analyzed by confocal microscopy to detect receptor (*red*) or lamin B_2 (*green*) localization. Images represent single optical sections of 0.4 μm merged such that *yellow* indicates co-localization of the specific antigens. *White lines* represent the positions of line scans across the cell diameter used for calculating the fluorescent emissions (intensity in arbitrary units) from subcellular structures; HA and LB_2 fluorescent traces are shown in *B. C,* analysis of line scan fluorescence. The average nuclear HA fluorescence (determined by co-localization with LB_2) was divided by an equivalent length (3 μm) of adjacent ER-localized HA fluorescence. The *y* axis reflects the NM/ER intensity ratio. *Bars* represent the mean ± S.E. of at least three independent replicates each with ratios from ≥15 cells/construct. The individual replicates per set of constructs are indicated by *triangles*, *squares,* and *diamonds* within the bar; **, $p < 0.01$. *D,* compiled data from immunohistochemistry results. ROI were selected from NM and PM using lamin B_2 staining and transmitted light images, respectively. NM HA intensity was divided by PM HA intensity; the *y* axis reflects the NM/PM intensity ratio. *Bars* represent the mean ± S.E. of at least three independent replicates each with ratios from ≥30 cells/construct. The individual replicates per set of constructs are indicated by *triangles, squares,* and *diamonds* within the bar; **, $p < 0.01$.

To further define which amino acids were responsible for nuclear targeting, we separately deleted amino acids 852–876 (Δ852–876) and amino acids 877–896 (Δ877–896) from the HA-tagged full-length mGluR5 plasmid (Fig. 4, *A* and *B*). HA immunostaining indicated that the Δ852–876 construct was largely in the ER, whereas Δ877–896 still showed strong co-localization with lamin B_2 (Fig. 4, *A* and *B*). Thus, these results suggest that amino acids 852–876 contain the minimal region for NM localization.

To determine whether these sequences were sufficient to target the nucleus on their own, we created a construct with an N-terminal Kozak sequence followed by mGluR5 amino acids

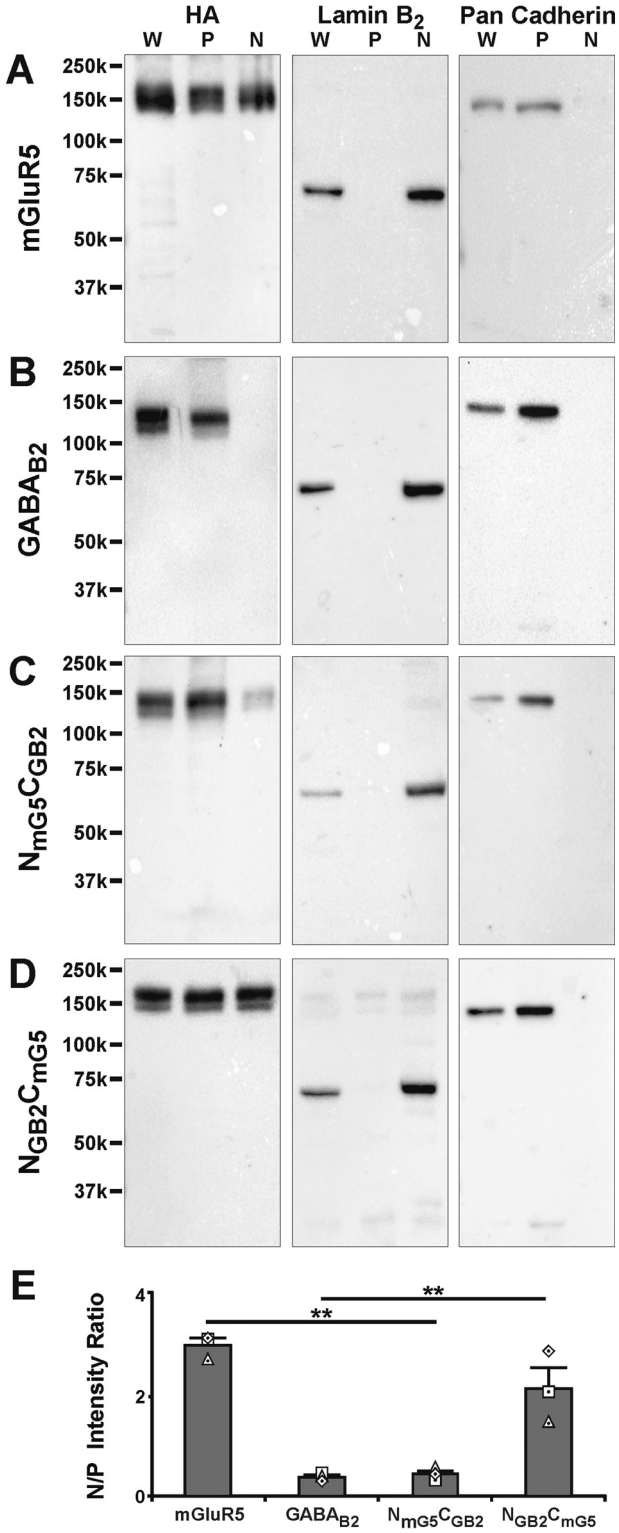

FIGURE 2. **Subcellular fractionation of HEK293 cells expressing mGluR5, $GABA_{B2}$, or the chimeric constructs confirms cellular distribution patterns.** Uncropped immunoblots of HA-tagged constructs, lamin B_2, and pan-cadherin show that only constructs expressing the mGluR5 C terminus can be detected in fractions containing both the nuclear (*N*) and plasma membranes (*P*) as well as in whole cells (*W*). *A–D,* molecular weights are indicated in the scale on the *left* of each construct panel. For all panels, 30 μg of protein from each fraction were separated on reducing SDS gels and transferred to nylon membranes. The blot was probed with antibodies against HA, lamin B_2, or pan-cadherin. *E,* quantitative analysis of western blotting results. Band intensities were measured, and nuclear (*N*) HA intensity was divided by the plasma membrane (*P*) HA intensity; the *y* axis reflects the N/P membrane intensity ratio. *Bars* represent the mean of three independent experiments ± S.E. The individual replicates are indicated by *triangles, squares,* and *diamonds* within the bar; **, $p < 0.01$.

827–992, an HA epitope, and then a stop codon. Because there are no transmembrane domains in this construct, it would not be associated with any membrane. However, if nuclear localization signals are found within this stretch of amino acids, then presumably karyopherins will recognize these motifs and promote the transport of the receptor fragment into the nucleoplasm. We also created new constructs, including the Δ852–876 deletion as well as the Δ877–896 deletion in the mG5 (827–992) backbone (Fig. 4*C*). As shown in Fig. 4, *C* and *D*, HA staining is only observed within the nucleus for constructs containing amino acids 852–876. In contrast, the construct missing those amino acids is largely found in the cytoplasm (Fig. 4, *C* and *D*). Therefore, these sequences contain sufficient information to be translocated into the nucleus.

To confirm and extend these results in a more physiological environment, we tested the localization of constructs in dissociated striatal neurons that endogenously express mGluR5. Thus, rat striatal neurons were transfected with the chimeric constructs, proximal mGluR5 constructs, or deletion constructs (mGluR5, $GABA_{B2}$, $N_{mG5}C_{GB2}$, $N_{GB2}C_{mG5}$, $N_{mG5\_854}C_{GB2}$, $N_{mG5\_896}C_{GB2}$, Δ852–876, and Δ877–896), subsequently immunostained, and then assessed for localization (Fig. 5, *A* and *B*). Lamin B_2 co-localization was observed for the $N_{GB2}C_{mG5}$, $N_{mG5\_896}C_{GB2}$, and Δ877–896 constructs, similar to what was observed in HEK293 cells. These data are consistent with mGluR5 requiring amino acids 852–876 for NM localization.

Distal C-terminal mGluR5 Sequences Do Not Play a Role in Nuclear Membrane Localization—To determine whether more distal mGluR5 C-terminal sequences also played a role in NM localization, we prepared additional constructs consisting of the entire $GABA_{B2}$ receptor fused with distal mGluR5 C-terminal stretches ($N_{GB2}C_{mG5\_827-966}$, $N_{GB2}C_{mG5\_967-1036}$, $N_{GB2}C_{mG5\_967-1106}$, and $N_{GB2}C_{mG5\_1107-1171}$). This strategy kept the total length of the chimeric C terminus at or below the original length of the mGluR5 C terminus. To compare all sequences within the same paradigm, we also tested the proximal mGluR5 C terminus by fusing the sequences 827–966 to the $GABA_{B2}$ tail ($N_{GB2}C_{mG5\_827-966}$; see Fig. 6*A*). Results confirmed that the mGluR5 C-terminal sequences 827–966 were able to re-direct the $GABA_{B2}$ receptor to intracellular membranes, including the NM, whereas distal mGluR5 C-terminal sequences did not affect $GABA_{B2}$ distribution (Fig. 6, *B–D*). This distribution pattern was also confirmed by subcellular fractionation (Fig. 7, *A–E*).

Activation of mGluR5 Chimeric Constructs Leads to Increased Cytoplasmic and Nucleoplasmic Ca^{2+}—To determine the functional response of the various mGluR5 proximal C-terminal constructs, we measured the following: 1) whole cell Ca^{2+} changes (Fig. 8); 2) IP_3 changes using targeted IP_3 sponges (Fig. 9); and 3) nuclear Ca^{2+} changes using isolated nuclei (Fig. 10). Bath application of mGluR5 agonists induced Ca^{2+} oscillations in HEK293 cells loaded with the Ca^{2+} indicator Oregon

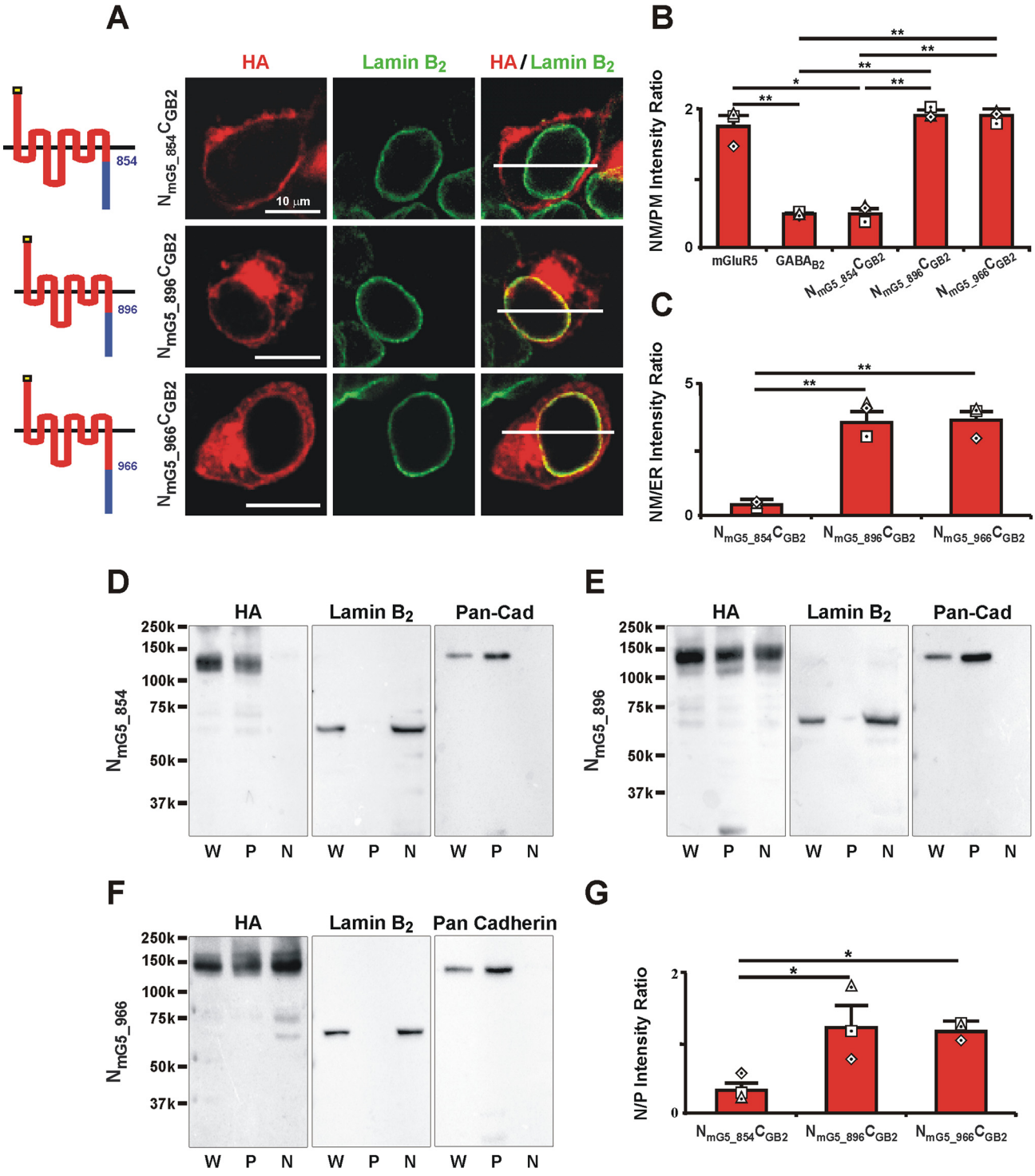

FIGURE 3. **mGluR5 C-terminal amino acids 855–896 are sufficient for nuclear membrane localization.** *A,* schematic illustration of the constructs that were transfected and tested for nuclear localization in HEK293 cells. *Yellow bars* indicate the HA tag; *red bars* indicate mGluR5; and *blue bars* indicate $GABA_{B2}$ receptor. *Numbers* indicate the last amino acid of the mGluR5 C terminus prior to fusion with the $GABA_{B2}$ intracellular C terminus (amino acids 741–940). HEK293 cells expressing the indicated constructs were fixed and processed for immunohistochemistry using HA and lamin B_2 antibodies. *Images* represent single optical sections of 0.4 μm merged such that *yellow* indicates co-localization of the specific antigens. *B,* quantitative analysis of immunohistochemistry results and comparison of the constructs with mGluR5 and $GABA_{B2}$. Averaged HA intensity measured from NM ROIs was divided by averaged HA intensity from PM ROIs; the *y* axis represents the NM/PM intensity ratio. *Bars* represent the mean ± S.E. of at least three independent replicates each with ratios from ≥30 cells/construct. The individual replicates per set of constructs are indicated by *triangles*, *squares*, and *diamonds* within the bar; **, $p < 0.01$; *, $p < 0.05$. *C,* compiled data from line scan profiles across diameters of cells transfected with indicated chimeric constructs and analyzed as in Fig. 1*C*; the *y* axis represents the NM/ER intensity ratio. *Bars* represent the mean ± S.E. of at least three independent replicates each with ratios from ≥15 cells/construct. The individual replicates per set of constructs are indicated by *triangles, squares,* and *diamonds* within the bar; **, $p < 0.01$. Subcellular fractionation of HEK293 cells expressing indicated constructs. *D–F* showed that $N_{mG5\_896}C_{GB2}$ and $N_{mG5\_966}C_{GB2}$ constructs can be detected in both PM (*P*) and NM (*N*) fractions as well as in whole cells (*W*). Gels and blots were probed as described under Fig. 2. *G,* quantitative analysis of western blotting results. Band intensities were measured, and nuclear (*N*) HA intensity was divided by the plasma membrane (*P*) HA intensity; the *y* axis represents the N/P intensity ratio. *Bars* represent the mean of three independent experiments ± S.E. The individual replicates are indicated by *triangles, squares,* and *diamonds* within the bar; *, $p < 0.05$.

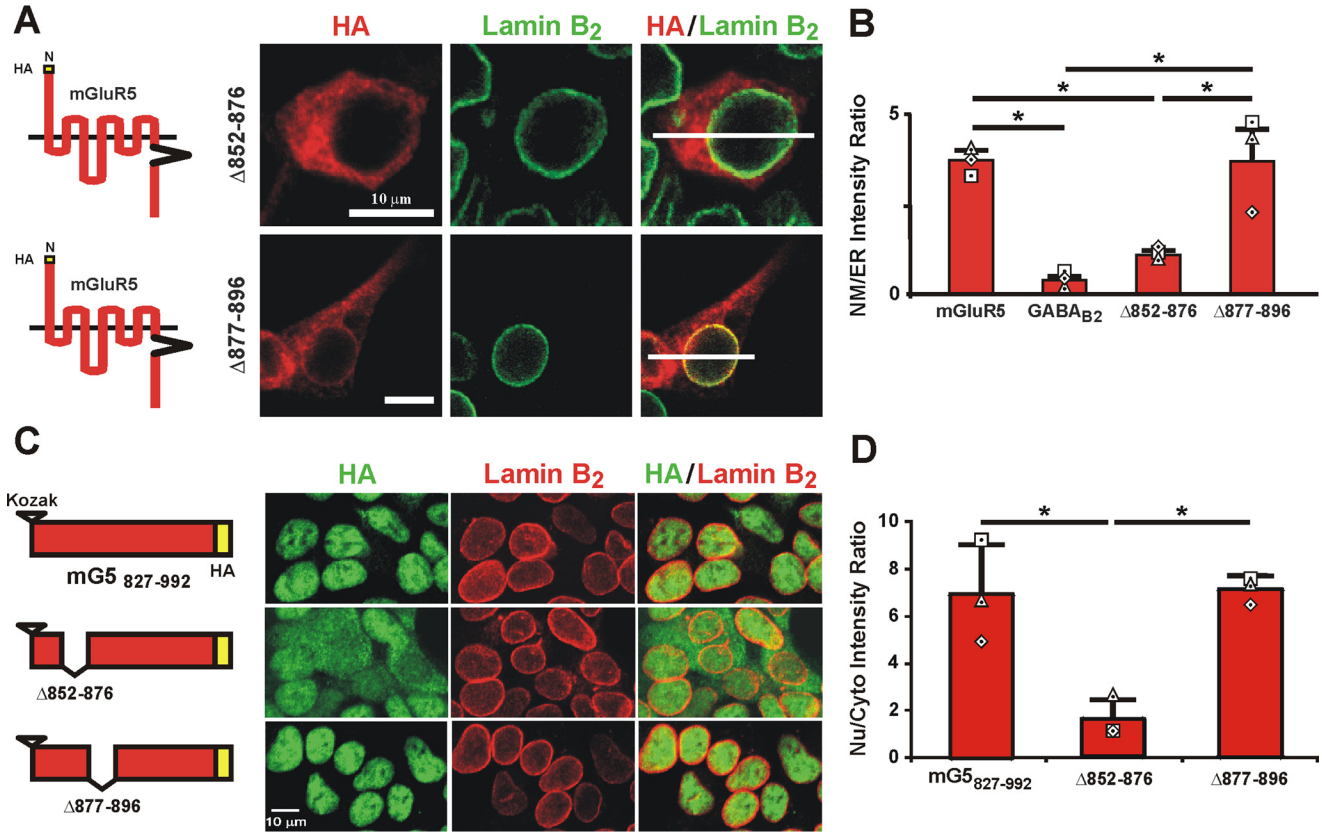

FIGURE 4. **mGluR5 C-terminal amino acids 852–876 are necessary and sufficient for nuclear membrane localization.** *A,* schematic illustration of deletion constructs Δ852–876 and Δ877–896. Transfected HEK cells were fixed and stained for HA-tagged receptors (*red*) and lamin B2 (*green*). Images represent single optical sections of 0.4 μm merged such that *yellow* indicates co-localization of the specific antigens. *White lines* represent the positions of line scans across the cell diameter used for calculating the fluorescent emissions from subcellular structures. *B,* compiled data from line scan profiles are analyzed as in Fig. 1*C*. The *y* axis represents the NM/ER intensity ratio. *Bars* represent the mean ± S.E. of at least three independent replicates each with ratios from ≥15 cells/construct. The individual replicates per set of constructs are indicated by *triangles, squares,* and *diamonds* within the bar; *, $p < 0.05$. *C,* mGluR5 C-terminal amino acids 827–992 localized to the nucleus. Schematic illustration of the truncated mGluR5 C-terminal construct with an N-terminal Kozak sequence, mGluR5 amino acids 827–992, the HA epitope, and a stop codon. The Δ852–876 and Δ877–896 deletions were also created in the mG5(827–992) backbone. Transfected HEK293 cells were fixed and stained using HA (*green*) and lamin B_2 (*red*) antibodies. *D,* ratio of the average intensity of nuclear HA fluorescence *versus* cytoplasmic HA fluorescence was quantified for each cell transfected with indicated chimeric constructs. *Bars* represent the mean ± S.E. of at least three independent replicates each with ratios from ≥50 cells/construct. The individual replicates per set of constructs are indicated by *triangles, squares,* and *diamonds* within the bar; *, $p < 0.05$.

Green BAPTA 1-AM whose spatio-temporal distribution was analyzed using real time confocal microscopy (30, 31). To activate cell surface mGluR5 and/or intracellular mGluR5, a combination of cell-permeant and -impermeant agonists and antagonists were utilized. Drug permeability was gauged using published lipophilicity values (LogP), in which values >2 are considered membrane-permeable (44). LogP values for quisqualate (−3.9), glutamate (−2.7), DHPG (−2.4), and LY393053 (0.6) are consistent with experimental evidence of membrane impermeability (31, 34–36). Thus, these agents cannot get into the cell unless there is an active transport/exchange process (19, 31, 34, 36). Using radiolabeled uptake studies, we have shown previously that quisqualate (Quis) and glutamate are transported into cells via sodium-dependent excitatory amino acid transporters and/or cysteine/glutamate exchangers (31). In contrast, neither DHPG nor LY393053 (LY53) is transported, although MPEP freely diffuses through membranes (LogP 3.3) (1, 19, 31, 34, 36). Thus, these compounds can pharmacologically isolate the cell surface from intracellular mGluR5 responses. Finally, although the chimeras contain the entire $GABA_{B2}$ tail, which couples to $G_{i/o}$ proteins, they also contain mGluR5 amino acids 827–850, which, together with the second intracellular loop, constitute the mGluR5 $G_{q/11}$-binding site (45, 46). Therefore, wild type and chimeric receptors couple to their normal signaling machinery.

Consistent with that prediction, transiently transfected HEK293 cells expressing $N_{mG5\_854}C_{GB2}$, $N_{mG5\_896}C_{GB2}$, or $N_{mG5\_966}C_{GB2}$ as well as mGluR5 as a positive control responded to either DHPG (Fig. 8, *A* and *B*), glutamate (Fig. 8, *C* and *D*), or Quis (Fig. 8, *E* and *F*) by generating stereotypic Ca^{2+} oscillations. Consistent with LogP values and data showing DHPG only activates cell surface receptors (31, 36), transfected cells pre-treated with the impermeable antagonist, LY53, did not respond to the impermeable agonist, whereas Quis application still triggered oscillatory responses (Fig. 8, *E* and *F*). Chimeric receptors did not show a significant difference in their oscillation amplitudes or frequencies in any drug application condition (Fig. 8, *B*, *D,* and *F,* and data not shown). These data indicate that all of the chimeric constructs are expressed on PM, ER, and at least the ONM where they couple to signaling systems generating changes in intracellular Ca^{2+} levels.

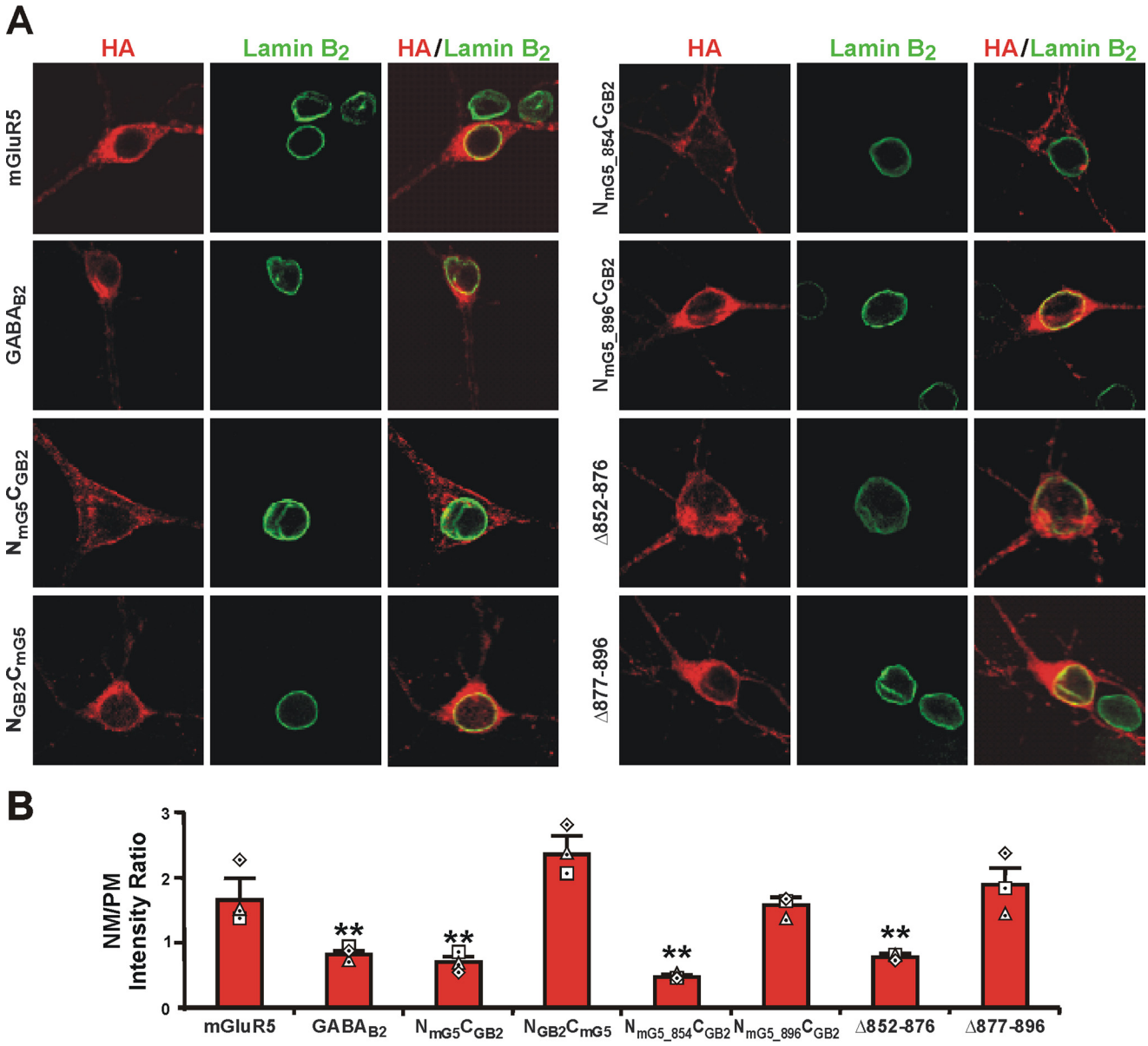

FIGURE 5. **mGluR5 C-terminal amino acids 852–876 are necessary for nuclear membrane localization in dissociated striatal neurons.** *A*, DIV5 rat striatal neurons were transfected with the indicated constructs, maintained in culture until DIV8, fixed, and processed for immunohistochemistry using HA and lamin B_2 antibodies. Cells were analyzed by confocal microscopy to detect receptor (*red*) or lamin B_2 (*green*) localization. Images represent single optical sections of 0.4 μm merged such that *yellow* indicates co-localization of the specific antigens. *B*, quantitative analysis of immunohistochemistry results of cells transfected with indicated chimeric constructs. Averaged HA intensity measured from NM ROIs was divided by averaged HA intensity from PM ROIs; the *y* axis represents the NM/PM intensity ratio. *Bars* represent the mean ± S.E. of at least three independent replicates each with ratios from ≥7 neurons/construct. The individual replicates per set of constructs are indicated by *triangles*, *squares* and *diamonds* within the bar; **, $p < 0.01$.

mGluR5 Amino Acids 852–876 Are Required for Inner Nuclear Membrane Functional Responses—Because both cell surface and intracellular mGluR5 can increase intracellular Ca^{2+} and as Ca^{2+} can enter the nucleoplasm thru the nuclear pore complex as well as via Ca^{2+} release channels on the nuclear envelope, it is difficult to assess whether one or both of those routes are being utilized following receptor activation. One way to overcome this limitation is use of a functional "sensor." In particular, we used a sensor incorporating an IP_3-binding site because this site has sufficient affinity to compete with the native receptor and therefore act like a "sponge" to remove IP_3 from its surroundings (47). Previously, we showed that nuclear mGluR5 couples to $G_{q/11}$ to activate nuclear phosphatidylinositol-phospholipase C, hydrolyze phosphatidylinositol 4,5-bisphosphate, and generate nuclear IP_3 (34), and thus a nuclearly targeted IP_3 binding domain fused with a fluorescent marker such as RFP would be predicted to block nucleoplasmic Ca^{2+} release due to nuclear mGluR5-mediated IP_3 production (Fig. 9*A*). Specifically, the nuclear IP_3 sponge with three NLS sequences will buffer IP_3 in the nucleus preventing nuclear Ca^{2+} signals from being generated; conversely, the cytoplasmic IP_3 sponge will buffer cytoplasmic IP_3 and prevent cytoplasmic Ca^{2+} responses (Fig. 9*A*) (48). In the case of wild type mGluR5, both sponge constructs showed the expected cellular distribution (Fig. 9*B*) as well as the predicted Ca^{2+}

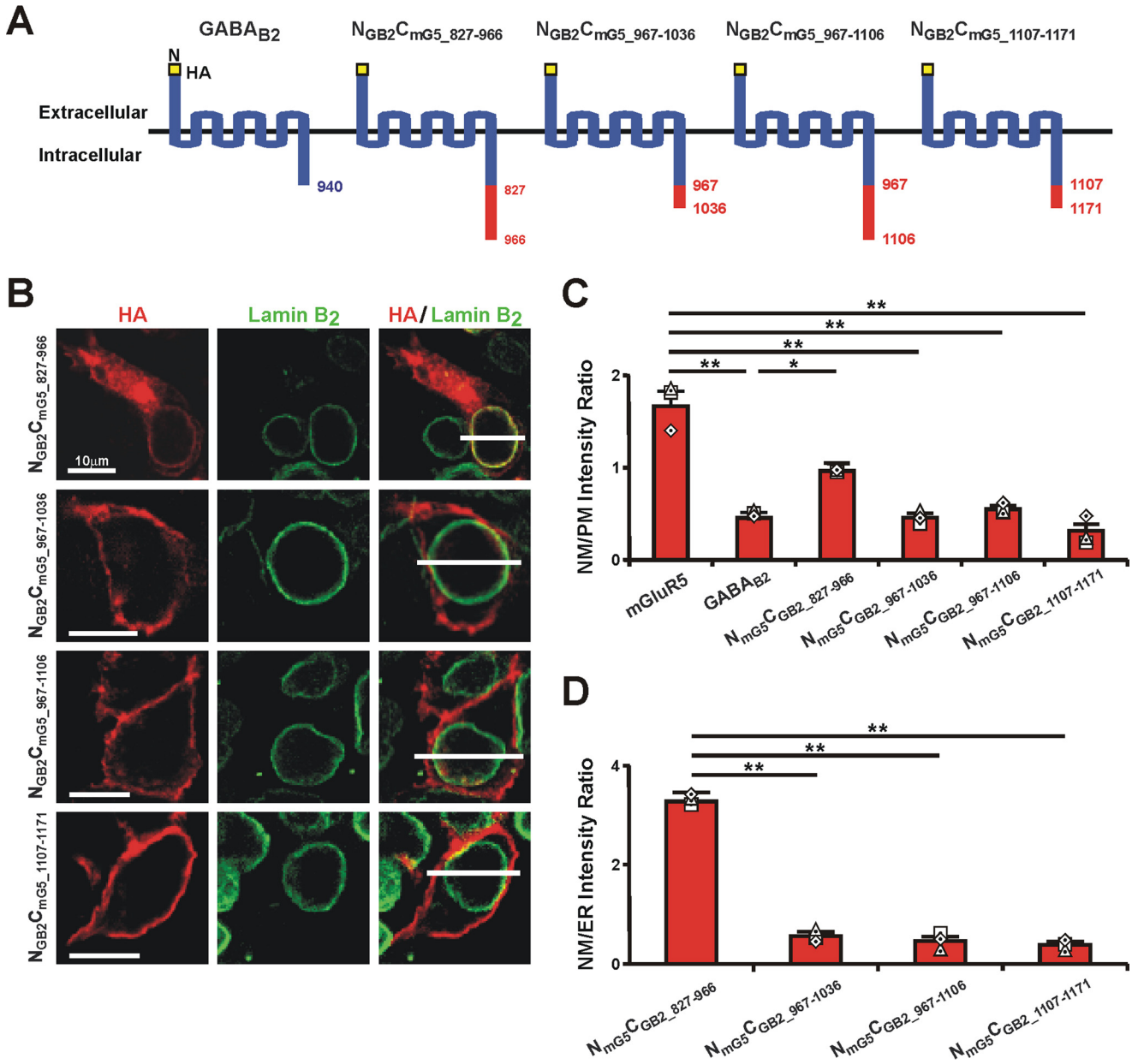

FIGURE 6. **mGluR5 C-terminal amino acids 967–1171 are not necessary for nuclear membrane localization.** *A,* schematic illustration of the constructs that were transfected and tested for nuclear localization in HEK293 cells. *Yellow bars* indicate HA tag; *red bars* indicate mGluR5; and *blue bars* indicate GABA$_{B2}$. *Numbers* indicate the first and the last amino acids of the mGluR5 C terminus added to the constructs. Note all constructs contain the entire GABA$_{B2}$ receptor plus or minus mGluR5 C-terminal fragments fused in-frame to the GABA$_{B2}$ C terminus. *B,* HEK293 cells were transfected with the indicated constructs, fixed, and processed for immunohistochemistry using HA and lamin B$_2$ antibodies. Cells were analyzed by confocal microscopy to detect receptor (*red*) or lamin B$_2$ (*green*) localization. Images represent single optical sections of 0.4 μm merged such that *yellow* indicates co-localization of the specific antigens. *White lines* represent the positions of line scans across the cell diameter used for calculating HA and LB$_2$ fluorescent emissions from subcellular structures. *C,* quantitative analysis of immunohistochemistry results and comparison of the constructs with mGluR5 and GABA$_{B2}$. HA intensity measured from NM was divided by PM HA intensity; the *y* axis represents the NM/PM intensity ratio. *Bars* represent the mean ± S.E. of at least three independent replicates each with ratios from ≥30 cells/construct. The individual replicates per set of constructs are indicated by *triangles, squares;* and *diamonds* within the bar; **, $p < 0.01$; *, $p < 0.05$. *D,* compiled data from line scan profiles from cells transfected with indicated chimeric constructs. Analysis of line scan fluorescence: the average nuclear HA fluorescence (determined by colocalization with LB$_2$) was divided by an equivalent length (3 μm) of adjacent ER-localized HA fluorescence. The *y* axis represents the NM/ER intensity ratio. *Bars* represent the mean ± S.E. of at least three independent replicates each with ratios from ≥15 cells/construct. The individual replicates per set of constructs are indicated by *triangles, squares,* and *diamonds* within the bar; **, $p < 0.01$.

response. Specifically, in the presence of glutamate, which will activate receptors on the cell surface, ER, ONM, and INM, Ca^{2+} responses were seen in both the cytoplasm and the nucleus in cells co-transfected with the nuclear or cytoplasmic IP_3 sponge (Fig. 9, *C* and *E*). In contrast, DHPG led to cytoplasmic Ca^{2+} oscillations in the presence of the nuclear IP_3 sponge but no oscillations when IP_3 was buffered using the cytoplasmic IP_3 sponge. This is consistent with DHPG not being taken up by the cell but instead activating cell surface receptors (Fig. 9, *D versus F*). Thus, the IP_3 sponge constructs confirm and extend our previous data showing that cell surface and intracellular mGluR5 generates intracellular Ca^{2+} responses.

Using this strategy, we determined the responses of $N_{mG5\_854}C_{GB2}$, $N_{mG5\_896}C_{GB2}$, and $N_{mG5\_966}C_{GB2}$ in the pres-

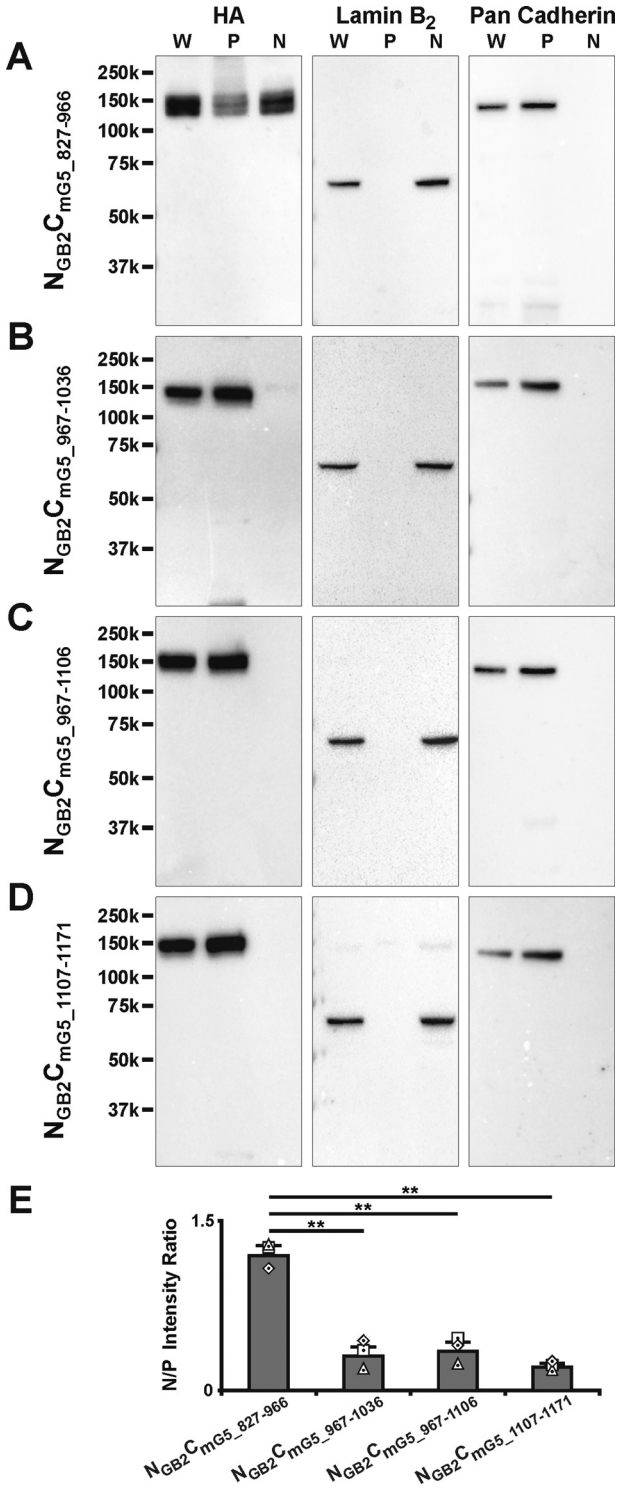

FIGURE 7. **Subcellular fractionation of HEK293 cells expressing mGluR5 C-terminal chimeric constructs.** mGluR5 amino acids 827–966 can partially localize $GABA_{B2}$ to the NM (*N*) *versus* PM (*P*) (*A*), whereas amino acids 967–1171 do not (*B–D*). Gels and blots were probed as described under Fig. 2. *E,* quantitative analysis of western blotting results. Band intensities were measured, and nuclear (*N*) HA intensity was divided by the plasma membrane (*P*) HA intensity. The *y* axis represents the N/P intensity ratio. *Bars* represent the mean of three independent experiments ± S.E. The individual replicates are indicated by *triangles, square,* and *diamonds* within the bar; **, $p < 0.01$. *W*, whole cells.

ence of either IP_3 sponge. Both sponge constructs exhibited the expected distribution in the presence of all chimeric constructs (data not shown) as well as equivalent transfection efficiencies (co-transfection efficiency was higher than 80% for all conditions; >250 cells counted/condition, $n = 3$).

Bath application of glutamate to cells co-transfected with $N_{mG5\_896}C_{GB2}$ and $N_{mG5\_966}C_{GB2}$ and either the NLS or NES IP_3 buffer construct generated the same results as the wild type mGluR5 clones (Fig. 9*I*). In contrast, co-expression of the NES IP_3 sponge with $N_{mG5\_854}C_{GB2}$ led to reduced Ca^{2+} generation in the cytoplasm, whereas the NLS IP_3 sponge did not inhibit cytoplasmic Ca^{2+} responses (Fig. 9*I*). Taken together, these data indicate that the chimeras containing sequences between 855 and 896 are present on the INM where they can affect the production of IP_3 and hence nucleoplasmic Ca^{2+}.

Although the IP_3 sponge data are consistent with $N_{mG5\_896}C_{GB2}$ and $N_{mG5\_966}C_{GB2}$ being present on the INM, they do not rule out the possibility that the observed Ca^{2+} fluctuations are due to other indirect causes. Given that only receptors present on INM could directly trigger nucleoplasmic Ca^{2+} responses in the presence of a nucleoplasmic Ca^{2+} fluorophore, we tested whether isolated nuclei expressing mGluR5/$GABA_{B2}$ proximal constructs would respond to bath application of glutamate as predicted from the NLS/NES IP_3 sponge experiments (Fig. 9). Isolated nuclei expressing wild type mGluR5 or $N_{mG5\_896}C_{GB2}$ exhibited Ca^{2+} oscillations in response to agonist application (Fig. 10, *A* and *C*), whereas $N_{mG5\_854}C_{GB2}$-expressing nuclei did not (Fig. 10*B*). Moreover, the mGluR5 deletion clones Δ852–876 could not generate Ca^{2+} oscillations in isolated nuclei and showed diminished Ca^{2+} oscillations when co-transfected with the NES IP_3 sponge, whereas Δ877–896 mirrored $N_{mG5\_896}C_{GB2}$ (data not shown). Collectively, these data indicate that sequences between mGluR5 amino acids 852 and 876 (SSAASRSSSLVNLWKRRGSSGETLS) are required for localization on the INM where such constructs can generate increased nucleoplasmic Ca^{2+}.

mGluR5 Goes through the Golgi to Get to the INM—Most transmembrane proteins are tagged with *N*-linked oligosaccharides as they are translocated through the ER membrane. These glycosylation groups are further modified as proteins move from the ER through the Golgi, and thus differential glycosylation can be used to monitor protein trafficking through these compartments. Specifically, *N*-linked glycosylation would be sensitive to Endo H digestion, whereas Endo H resistance suggests a protein has been trafficked at least to the *cis/medial*-Golgi where PNGase F can remove all *N*-linked glycans. mGluR5 has six putative *N*-glycosylation sites, although only one (Asn-444) appears to be utilized (49). By treating plasma membrane preparations with both enzymes and comparing the resulting immunoblots with non-treated protein, we observed an mGluR5 mobility shift akin to what was previously reported following PNGase F but not Endo H treatment (Fig. 11*A*). When nuclear membrane preparations were treated with Endo H and PNGase F, similar results were observed, although occasionally small amounts of nuclear protein appeared to be sensitive to Endo H treatment (~7.5% of total). These data indicate that >90% of mGluR5 is processed through the Golgi ruling out simple ER diffusion to the INM.

INM mGluR5 Does Not Originate at the PM—If INM mGluR5 is not diffusing from the ER, then perhaps like the apelin, angiotensin, and F2rl1 GPCRs, mGluR5 is being routed

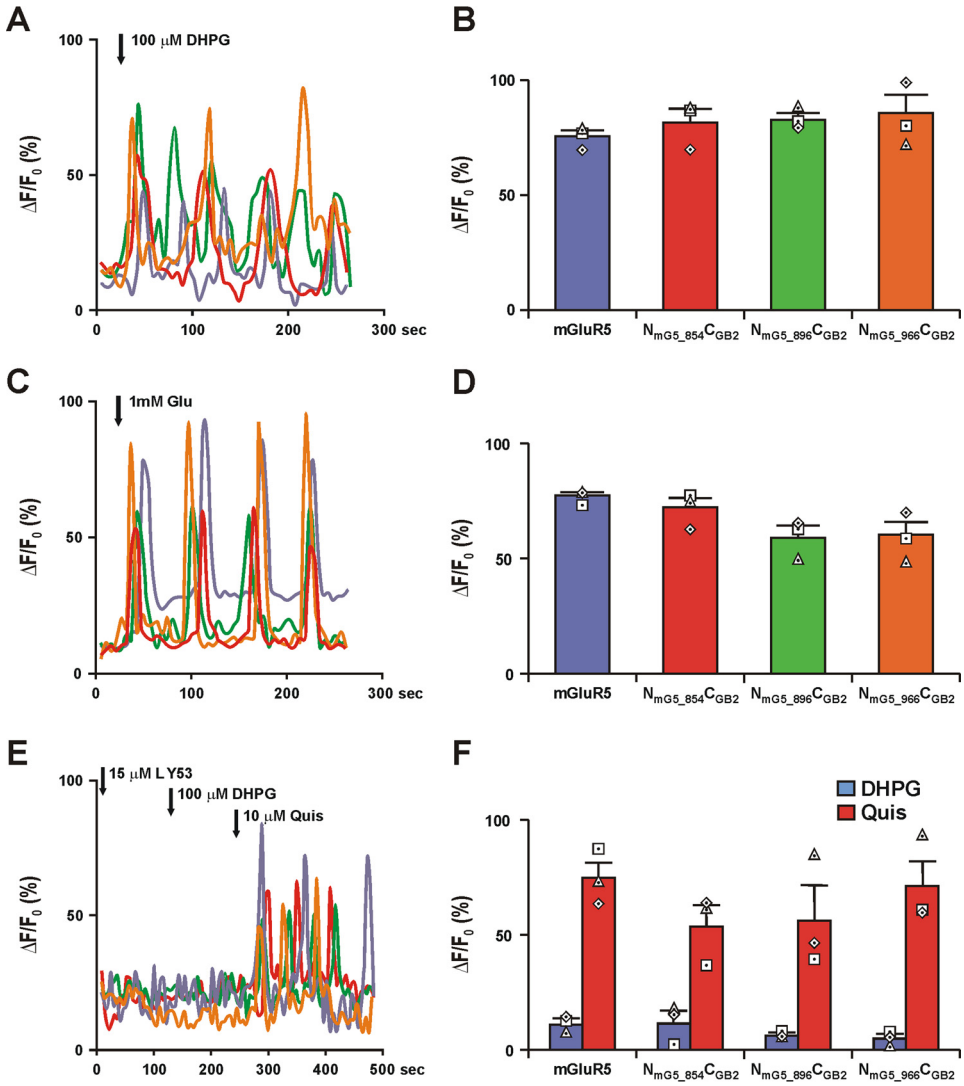

FIGURE 8. **Activation of mGluR5 chimeric constructs leads to increased cytoplasmic Ca^{2+}.** mGluR5 (*blue*), $N_{mG5\_854}C_{GB2}$ (*red*), $N_{mG5\_896}C_{GB2}$ (*green*), and $N_{mG5\_966}C_{GB2}$ (*orange*) constructs were transiently expressed in HEK293 cells, loaded with Oregon Green BAPTA AM (30), and then monitored in real time following bath addition of the indicated ligands. *A,* representative fluorescent traces after 100 μM DHPG. *B, bars* represent compiled data from the mean ± S.E. of the maximum response of the initial peak ($\Delta F/F_0$) from three independent replicates each with ratios from ≥30 cells/construct. The individual replicates per set of constructs are indicated by *triangles, squares,* and *diamonds* within the bar. *C,* traces following 1 mM glutamate (*Glu*). *D,* compiled data as described in *B*. *E,* representative traces following serial addition of drugs. To isolate the intracellular receptor, response cells were pretreated with the impermeable non-transported antagonist LY53 (15 μM), which blocked the impermeable, non-transported DHPG-induced Ca^{2+} responses but not the transported Quis-induced Ca^{2+} responses. *F,* compiled data as described above from maximal DHPG and Quis responses. No significant differences were observed between the constructs.

from the PM to the INM. Although canonical NLS motifs are not apparent in the mGluR5 C-terminal domain (50, 51), there are three consecutive basic amino acids (KRR) between 852–876, the region defined as required for INM localization. However, mutating these sequences to QQQ had no effect on mGluR5 localization (data not shown). Thus, these data suggest that no canonical NLS or derivation thereof is responsible for the INM localization of mGluR5. Instead, other sequences and/or mechanisms must be a factor.

Because apelin, angiotensin, and F2rl1 translocate to the nucleus upon receptor activation (13–16), we tested whether glutamate treatment of mGluR5 stable HEK cells led to increased levels of receptors on nuclear membranes following subcellular fractionation. Even after 1 h of glutamate treatment, no significant differences were seen in mGluR5 levels on nuclear membranes following vehicle, glutamate-treated, or MPEP/glutamate-treated samples (Fig. 11*B*).

To more directly examine whether PM mGluR5 could traffic to nuclear membranes, we constructed the 13-amino acid bungarotoxin-binding site (BBS) within the mGluR5 extracellular domain (Fig. 11*C*). The BBS is recognized by its high affinity ligand, bungarotoxin, which when conjugated with rhodamine allows the labeled receptor to be tracked via imaging techniques (52). Bungarotoxin-labeled mGluR5 was followed for 1 h with or without glutamate treatment. Although PM signals gradually dimmed, no label was ever observed at the nuclear membrane. Rather, internalized puncta were observed near the PM within 10 min of labeling after which they disappeared (Fig. 11*C*). In agreement with a previous study using Myc-tagged mGluR5 (53), the addition of ligand accelerated the internaliza-

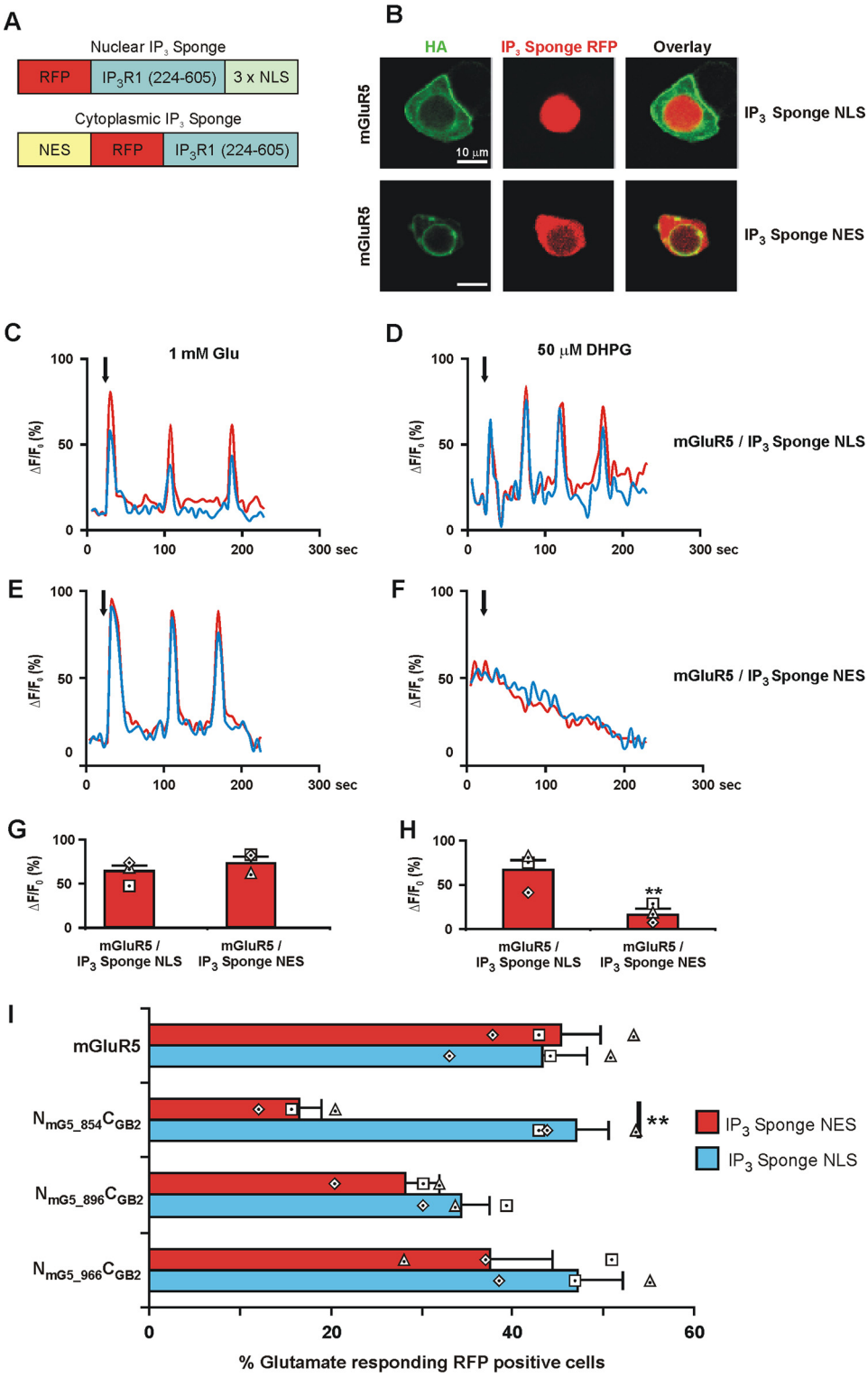

FIGURE 9. **Cytoplasmic IP_3 sponge construct blocks Ca^{2+} response of $N_{mG5\_854}C_{GB2}$-transfected HEK293 cells.** *A*, schematic representation of RFP-tagged IP_3 sponge constructs: *NES*, nuclear exclusion signal; *NLS*, nuclear localization signal; $IP_3R1(224–605)$, IP_3 binding domain of the human type I IP_3 receptor (*IP_3R1*). *B*, representative images showing expression of IP_3 sponge NLS or IP_3 sponge NES with mGluR5 in HEK293 cells. HA staining indicates mGluR5 expression, and RFP signal indicates IP_3 sponge construct expression. *C–F*, representative traces are shown of cytoplasmic (*blue line*) or nuclear (*red line*) Ca^{2+} responses from HEK293 cells co-transfected with mGluR5 and IP_3 sponge NLS constructs (*C* and *D*) or mGluR5 and IP_3 sponge NES constructs (*E* and *F*) following bath addition of 1 mM glutamate (*C* and *E*) or 50 μM DHPG (*D* and *F*) at indicated points. *G* and *H*, *bars* represent compiled data from the mean ± S.E. of the maximum response of the initial peak ($\Delta F/F_0$) from three independent replicates each with ratios from ≥30 cells/indicated construct and activated by glutamate (*G*) or DHPG (*H*). The individual replicates per set of constructs are indicated by *triangles, squares,* and *diamonds* within the bar; **, $p < 0.01$. *I*, compiled data from HEK293 cells expressing each construct (mGluR5, $N_{mG5\_854}C_{GB2}$, $N_{mG5\_896}C_{GB2}$, or $N_{mG5\_966}C_{GB2}$) with either the cytoplasmic IP_3 sponge (*red bars*) or the nuclear IP_3 sponge (*blue bars*). *Bars* represent the percentage of RFP-positive cells that also exhibited a glutamate-induced Ca^{2+} response. *Bars* represent the mean ± S.E. from three independent replicates each with ratios from ≥30 cells/construct. The individual replicates per set of constructs are indicated by *triangles, squares,* and *diamonds* within the bar; **, $p < 0.01$.

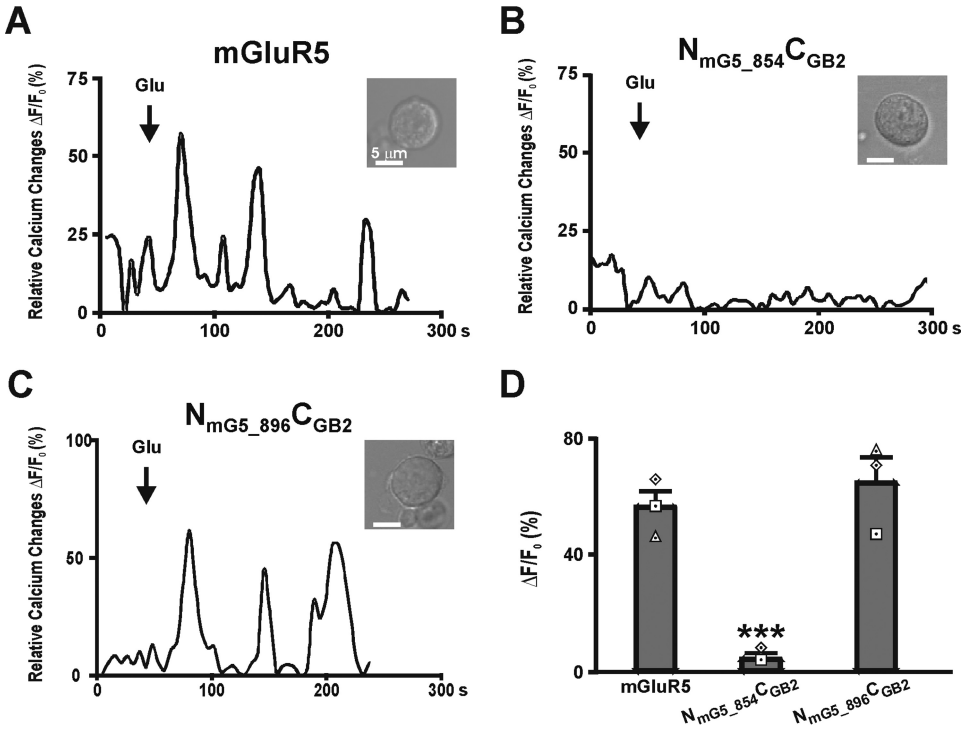

FIGURE 10. **Glutamate-mediated Ca^{2+} changes in isolated nuclei.** Nuclei (transmitted light images in *upper right corner*) were isolated from mGluR5-, $N_{mG5\_854}C_{GB2}$-, or $N_{mG5\_896}C_{GB2}$-transfected cells, loaded with Oregon Green BAPTA, and treated at indicated times with 1 mM glutamate (*Glu*). *A*, representative trace of Glu-mediated Ca^{2+} oscillations in nucleus-expressing mGluR5. *B*, trace from $N_{mG5\_854}C_{GB2}$-expressing nucleus. *C*, $N_{mG5\_896}C_{GB2}$-expressing nucleus. *D*, *bars* represent compiled data from the mean ± S.E. of the maximum response of the initial peak ($\Delta F/F_0$) from three independent replicates each with ratios from ≥10 nuclei/construct. The individual replicates per set of constructs are indicated by *triangles, squares,* and *diamonds* within the bar. $N_{mG5\_854}C_{GB2}$-expressing nuclei never exhibited Ca^{2+} oscillations in three independent experiments whereas mGluR5- and $N_{mG5\_896}C_{GB2}$-expressing nuclei were always positive. ***, $p < 0.001$; $N_{mG5\_854}C_{GB2}$ is significantly different from mGluR5; no significant (*n.s.*) difference between mGluR5 and $N_{mG5\_896}C_{GB2}$.

tion of mGluR5, although its presence on the nuclear membrane was never observed (Fig. 11*D*). These data suggest that PM-localized mGluR5 is not the initiating source for NM-localized mGluR5. Rather, internalized receptors were either degraded or recycled back to the PM (53).

mGluR5 C-terminal Domain Interacts with Chromatin—Previously, immunogold staining with antibodies directed against the C-terminal portion of mGluR5 showed the presence of many immunogold particles associated with electron-dense material close to the INM representing chromatin (30, 34). Moreover, mGluR5 amino acids 827–896 have a pI of 11.64, and those of the defined INM domain (854–896) have a pI of 11.71. Conceivably, such an overall positive charge might promote interactions with the negatively charged chromatin (54). To directly test the hypothesis that the mGluR5 C-terminal tail interacts with DNA, we cross-linked putative nucleic acids to transiently expressed mGluR5 and $GABA_{B2}$ receptors and then immunoprecipitated DNA using HA antibodies. To amplify precipitated DNA, we used primers recognizing the human repetitive DNA sequence, Alu (55). Precipitated material from mGluR5-expressing cells but not $GABA_{B2}$ led to DNA amplification (Fig. 12*A*) suggesting that mGluR5 interacts with DNA. Moreover, we could pull down DNA from the cells expressing $N_{mG5\_896}C_{GB2}$ receptor but not $N_{mG5\_854}C_{GB2}$ receptor, further suggesting the importance of amino acids 855–896 for INM localization and retention (Fig. 12, *A* and *B*).

INM mGluR5 Exhibits Low Mobility whereas ER-localized mGluR5 Moves Rapidly in the Membrane—INM proteins exhibit very little movement presumably due to their tethering to the chromatin. Consistent with this hypothesis, photoconversion of dendra-tagged mGluR5 on the NM also revealed a very stationary protein akin to the LBR (Fig. 13, *A* and *B*). In contrast, photoconversion of dendra-tagged mGluR5 in the ER revealed rapid movement throughout the cytoplasm (Fig. 13, *A* and *B*). We also used FRAP to assess mGluR5 mobility at the nuclear membrane and again found that like INM LBR the mGluR5 immobile fraction was >50%, whereas on ER membranes both mGluR5 and LBR were highly mobile (Fig. 13, *C* and *D*). Taken together, these data confirm the notion that mGluR5 is not freely mobile at the INM but rather is anchored in place presumably via its chromatin interactions (Fig. 13*E*).

Discussion

Although many GPCRs are localized at the INM, the signals responsible for either trafficking or retaining these receptors in this locale are just emerging. Using optical, molecular, and pharmacological techniques, here we show that sequences between 852 and 876 of mGluR5 are necessary and sufficient for targeting this receptor to the INM. Because these sequences do not correspond to any known NLS (50, 51), they represent a new motif for INM trafficking. mGluR5 is also trafficked to the PM where it undergoes re-cycling/degradation in a separate receptor pool, one that does not interact with the nuclear mGluR5 pool. Finally, our data suggest that once at the INM, mGluR5 is stably retained via interactions with the chromatin. Thus, mGluR5 is perfectly positioned to regulate nucleoplasmic Ca^{2+} *in situ*.

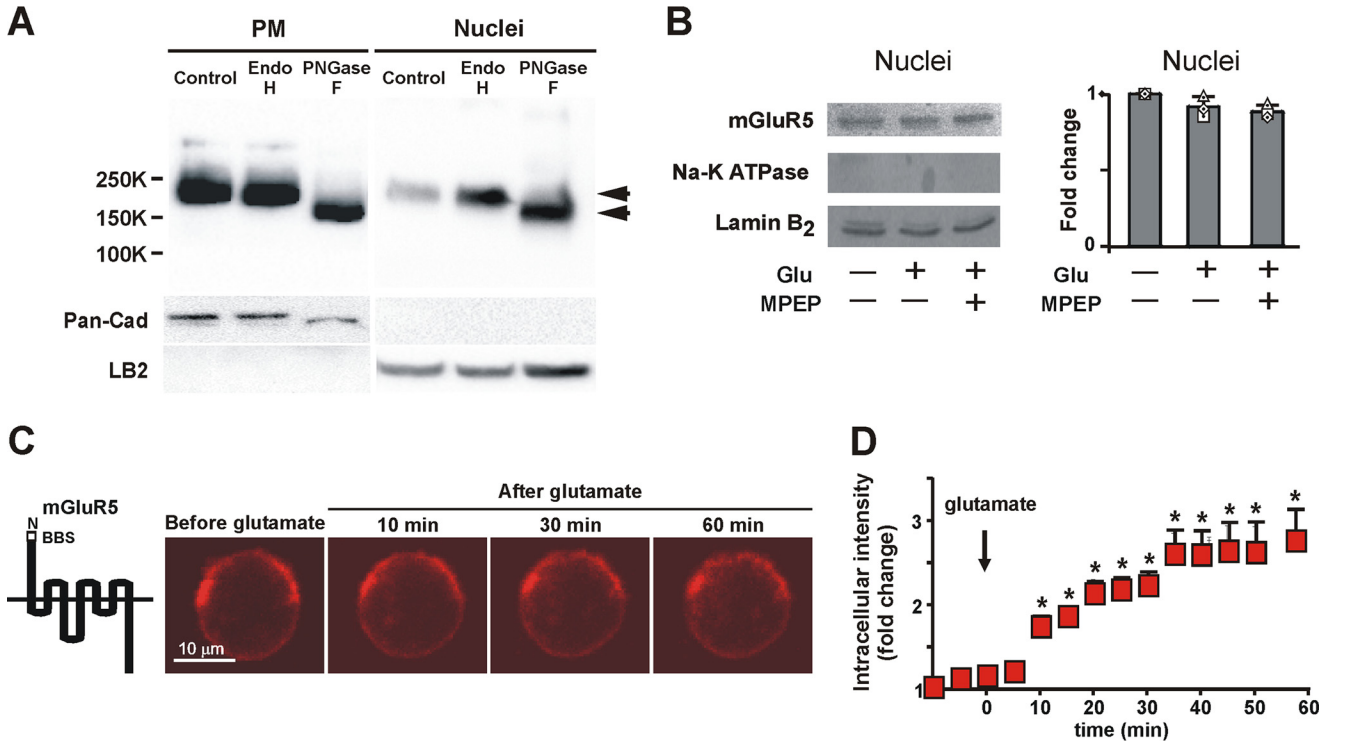

FIGURE 11. **mGluR5 trafficking in HEK cells.** *A,* glycosylation analysis of mGluR5 in subcellular fractions of either PM or nuclei derived from mGluR5-expressing HEK cells. Control, Endo H-, or PNGase F-treated membrane fractions were analyzed using SDS-PAGE and western blotting with anti-mGluR5. PM and nuclear membrane fractions primarily contained Endo H-resistant mGluR5; long exposures showed a small amount of nuclear mGluR5 (~7.5% of total) was sensitive to Endo H treatment. *B,* fractionated nuclei from mGluR5-expressing HEK cells treated with vehicle, 1 mM Glu, or pre-treated with 10 μM MPEP followed by 1 mM Glu for 1 h. Thirty micrograms of protein from each fraction were separated on reducing SDS gels and transferred to nylon membranes. The same blot was sequentially probed with antibodies against HA, lamin B_2, and pan-cadherin antibody. Quantitative analysis of western blotting results showed no significant difference across all treatments. *Bars* represent the mean of three independent experiments ± S.E. The individual replicates are indicated by *triangles, squares,* and *diamonds* within the bar. *C,* internalization of fluorescent bungarotoxin-tagged mGluR5 after 1 mM glutamate treatment of transiently transfected HEK cells expressing mGluR5 containing a BBS. Static images at indicated times after glutamate addition. *D,* internalization of fluorescently labeled mGluR5 was followed in real time. Data from the mean ± S.E. from 14 independent replicates. *, $p < 0.05$.

The requirement of the 852–876 region for INM localization is supported by a number of observations. First, two mGluR5 constructs, $N_{mG5\_896}C_{GB2}$ and $N_{mG5\_966}C_{GB2}$, which encompass this region (855–896), were detected on NMs via immunocytochemical and fractionation analysis, but the Δ852–876 deletion construct was not detected in either HEK293 cells or striatal neurons (Fig. 4, 5). Second, both cytoplasmic and nuclear IP_3 sponge constructs did not block the Ca^{2+} responses of $N_{mG5\_896}C_{GB2}$ and $N_{mG5\_966}C_{GB2}$ receptors, although the cytoplasmic IP_3 sponge blocked the Ca^{2+} response of $N_{mG5\_854}C_{GB2}$ (Fig. 9). Third, nuclei isolated from $N_{mG5\_896}C_{GB2}$- and Δ877–896-expressing HEK293 cells responded to the agonist glutamate and generated nucleoplasmic Ca^{2+} oscillations but $N_{mG5\_854}C_{GB2}$ and Δ852–876 expressing nuclei did not (Fig. 10, not shown). Fourth, chromatin immunoprecipitation revealed a specific DNA interaction between amino acids 855–896 but not for amino acids 827–854 or $GABA_{B2}$ receptors (Fig. 12). Finally, >90% of nuclear mGluR5 exhibits a mature glycosylation pattern indicative of trafficking through the Golgi (Fig. 11*A*), which makes immediate lateral diffusion from the ER to the ONM to the INM unlikely. Rather, these data support a model in which the C-terminal domain of mGluR5 is translocated to the INM via non-canonical transport mechanisms and subsequently is retained by chromatin interactions (Fig. 12).

Unlike the movement of soluble proteins from the cytoplasm into the nucleus, there appear to be many mechanisms associated with INM protein translocation. These range from lateral diffusion through peripheral channels to movement through the nuclear pore complex using linkers, carrier proteins, and even known components of the soluble transport machinery (20, 21). For example, certain GPCRs such as the apelin, angiotensin AT1, and bradykinin B2 receptors use a canonical NLS for nuclear import (13). Indeed, the F2rl1 receptor translocates from the PM to the NM via importin β1 and sorting nexin Snx11 (16). However, unlike these receptors, mGluR5 has only a very small stretch of basic amino acids (KRR) in its C-terminal sequence, which when mutated did not block INM localization (data not shown). Even though the KRR sequence was not involved in INM trafficking, sequences encompassing the INM domain were sufficient to localize to the nucleoplasm after transfection (Fig. 4, *C* and *D*). The latter finding indicates that other motifs within the INM sequence are recognized by translocation machinery allowing it to be carried to the nucleus. Thus, despite precedence for known NLS sequences being involved in transporting GPCRs to the nucleus, mGluR5 does not use any of the classical motifs (56) to arrive at the INM.

Another feature of mGluR5 INM localization is that it does not appear to originate at the PM. In agreement with earlier observations (53, 57, 58), mGluR5 undergoes constitutive inter-

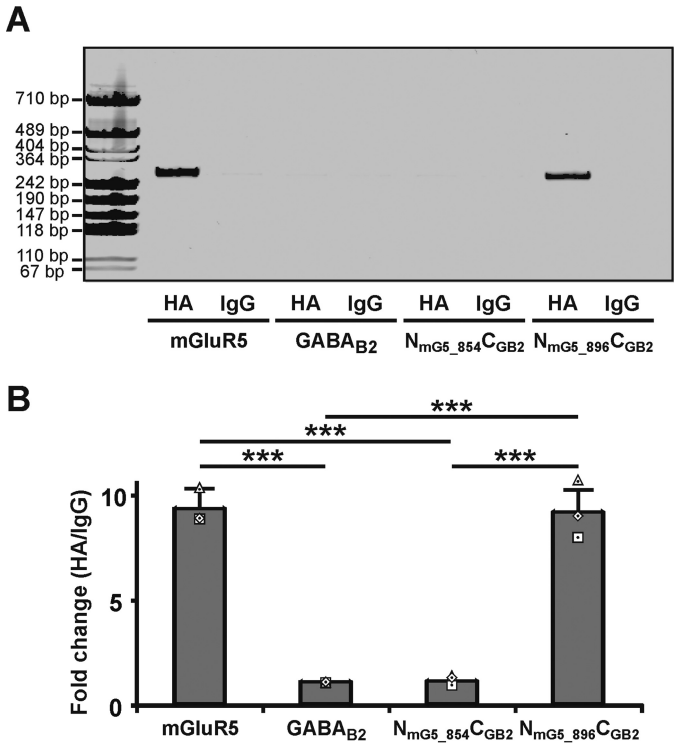

FIGURE 12. **mGluR5 C terminus interacts with chromatin.** *A,* CHIP analysis of HEK293 cells expressing either mGluR5, GABA$_{B2}$,N$_{mG5_854}$C$_{GB2}$, or N$_{mG5_896}$C$_{GB2}$. As indicated previously, all constructs are tagged with the HA epitope. Therefore, samples were immunoprecipitated with either HA or nonspecific IgG antibodies. PCR analysis of eluted DNA was done by using oligonucleotides specific for human repetitive DNA sequence Alu. DNA interaction was detected for mGluR5 and N$_{mG5_896}$C$_{GB2}$ construct but not GABA$_{B2}$ and N$_{mG5_854}$C$_{GB2}$. *B,* quantitation of CHIP results in *A*. The ratio of PCR product intensity of HA immunoprecipitation *versus* nonspecific IgG immunoprecipitation of each indicated chimeric construct was quantified. *Bars* represent the mean of three independent experiments ± S.E. The individual replicates are indicated by *triangles, squares,* and *diamonds* within the bar; ***, $p < 0.001$.

nalization in the absence of ligand, a process that is significantly enhanced after glutamate treatment (Fig. 11, *C* and *D*). Despite this ongoing internalization, at no time did rhodamine-labeled mGluR5 appear at the nuclear membrane. Instead, structures akin to the recycling compartments identified by Trivedi and Bhattacharyya (53) were apparent 30 min after initiation of internalization (Fig. 11). Trivedi and Bhattacharyya (53) also showed that mGluR5 is subsequently recycled back to the PM within 2 h. Thus, in their study and this one, mGluR5 underwent internalization and recycling as a seemingly "PM-centric" receptor pool, not one associated with the NM. Consistent with these data, nuclei purified 1 h after glutamate treatment of mGluR5 HEK cells did not show increased levels of mGluR5 in nuclear fractions nor were there increased numbers of receptors (Fig. 11*B*). Moreover, photoconversion of dendra-tagged mGluR5 showed diffusion only along the PM and in nearby puncta; there were no photoconverted (red) puncta in perinuclear or INM locations (data not shown). These data suggest that the nuclear mGluR5 receptor pool is distinct from the PM pool.

Because nuclear mGluR5 contains complex glycans (Fig. 11*A*), it must be processed at least as far as the *cis/medial*-Golgi compartment and possibly to the *trans*-Golgi network as well (59). In either case, membrane traffic between the ER and the Golgi is bidirectional and highly dynamic (59). Consistent with its presence on PM and the nucleus, there are no sequences within mGluR5 that have been described to serve as "retrieval" motifs (21), *i.e.* sequences that might be involved in retrograde trafficking from the Golgi to the ER. Similarly, INM sorting motifs such as KTKK, KKLK, or KKSSK (21) are not apparent either within the mGluR5 INM localization domain or C-terminal tail. The lack of destination or retrieval motifs may contribute to our finding that mGluR5 is present on all of these membranes *versus* being entirely localized on one. These data support a more dynamic diffusion model, one in which mGluR5 is cycled from the Golgi to the ER and then undergoes either simple lateral diffusion or a facilitated process to reach the INM.

At its simplest, lateral diffusion is thought to involve translocation through the peripheral channels of the nuclear pore complex. Because of the size constraints of these channels, the nucleoplasmic domains of INM proteins must be under 60 kDa (25–27). Because the C-terminal domain of mGluR5 is 35 kDa (60), it is well below the predicted limit (20). However, tandem copies of the mGluR5 C-terminal tail would be above the limit, and in fact, increasing the size of the nucleoplasmic domain by doubling the C terminus prevented mGluR5 from getting to the INM (data not shown). Thus, at least by these criteria, it appears that mGluR5 goes through the peripheral channels.

Recent data have expanded the mechanisms involved in INM localization. For example, some INM proteins go through peripheral channels using facilitator proteins, some require ATP, and certain INM proteins help themselves via phenylalanine-glycine (FG) interactions with particular nuclear pore proteins (*e.g.* Nup 35 (20)). Because the mGluR5 C terminus contains no FG motifs, the latter mechanism seems unlikely. Although some transmembrane-spanning proteins get to the INM via the central pore possibly with the aid of a linker protein (21), the most parsimonious pathway based on current data is that mGluR5 translocates via the peripheral channel with or without the help of a facilitator protein.

Interactions between INM proteins and nuclear resident proteins and/or chromatin are thought to complete the INM localization process (22). Because diffusion could go either way, tethering the proteins on one side would provide directionality to the process. For example, INM proteins such as Emerin, LBR, Lamin-associated polypeptide (Lap)1, Lap2, and Man1 are all tethered to the INM via lamin interactions (61, 62). LBR also binds to the chromatin suggesting that nucleic acids can also function in this capacity (63, 64). Our current data suggest that the chromatin plays a role in the INM localization of mGluR5 (Fig. 11). By analogy with LBR, which interacts with chromatin via a basic region (pI >9.8) (54, 65, 66), the mGluR5 INM localization domain is also very basic, which may promote its chromatin interaction (Fig. 12).

Finally, various studies have indicated that different C-terminal interacting proteins can re-direct mGluR5 to a particular membrane. For example, Homer or Tamalin take mGluR5 to the somal or dendritic membranes of particular neurons (67). Another recently described protein, Norbin, has also been shown to enhance the presence of mGluR5 on the PM (68). Interestingly, there are two Norbin-binding sites in the mGluR5

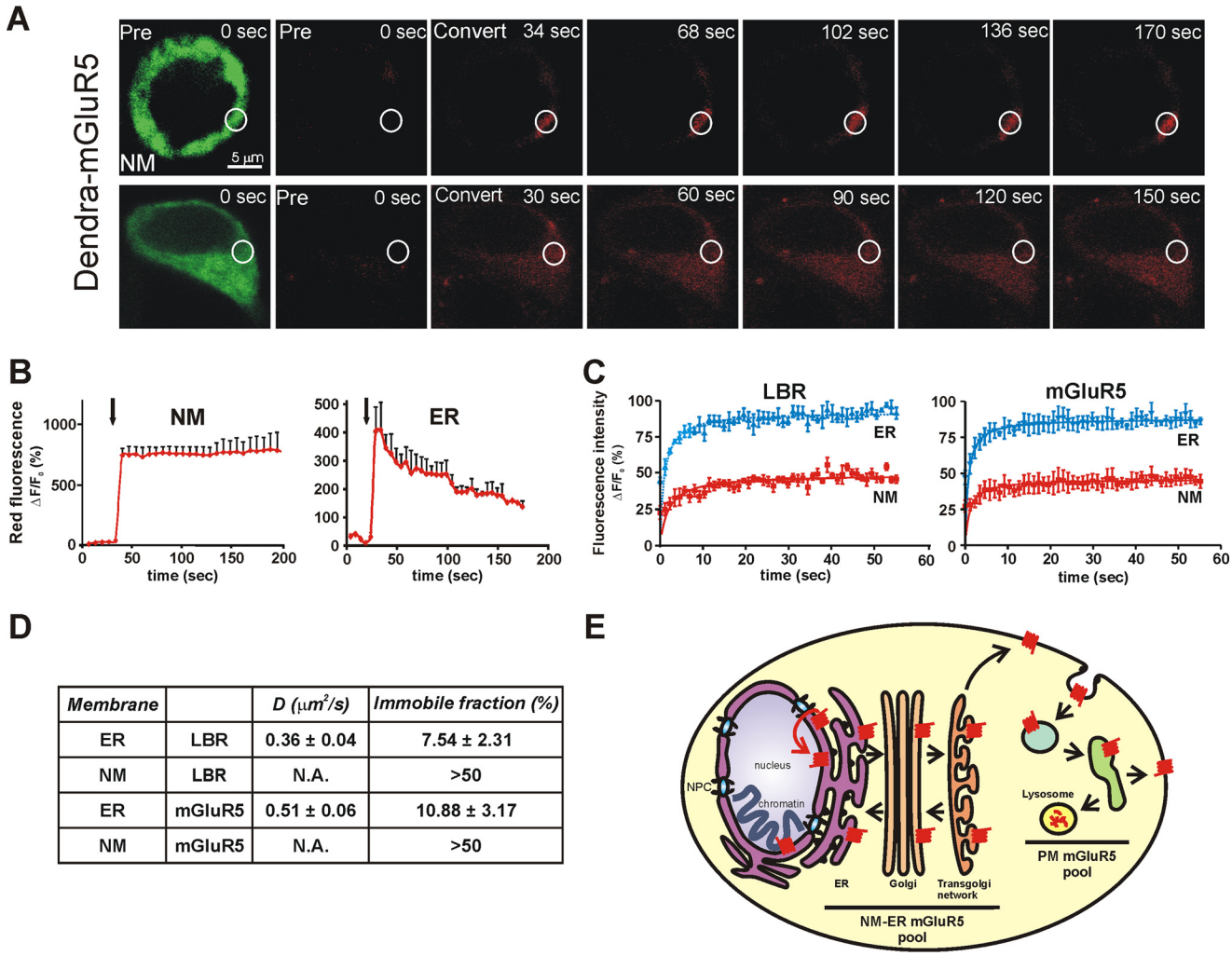

Membrane		*D* (μm²/s)	*Immobile fraction (%)*
ER	LBR	0.36 ± 0.04	7.54 ± 2.31
NM	LBR	N.A.	>50
ER	mGluR5	0.51 ± 0.06	10.88 ± 3.17
NM	mGluR5	N.A.	>50

FIGURE 13. **mGluR5 is immobilized on NMs.** *A,* dendra-tagged mGluR5 is almost stationary on NMs, whereas it is highly mobile in the ER of transiently transfected HEK cells. Representative images showing ROIs (*white circles*) in isolated NMs (*upper panel*) or whole cell ER (*lower panel*) before and after photoconversion. *B,* quantitation of dendra-mGluR5 movement in NM and ER membranes. Background-subtracted mean fluorescence intensities/area are plotted against time for each of the outlined ROIs on either ER or nuclear membranes. Data are the mean of three independent experiments ($n = 5$ cells). *C,* quantitative FRAP experiments to determine diffusion coefficients for tagged LBR and mGluR5. Fluorescent intensities after photobleaching were plotted at 1.12-s intervals until plateauing. Fluorescence was normalized to prebleach intensity corrected for the total loss of fluorescence due to high energy laser bleaching, $I_o = 100$ (normalized prebleach intensity). Recovery at $t = 60$ s was used as a measure of the mobile fraction of molecules. *D,* diffusion coefficients (D; $\mu m^2/s$)) and immobile fractions (%) of LBR-GFP and mGluR5-GFP. The diffusion coefficient and ER immobile fraction of tagged LBR were not significantly different from the diffusion coefficient and ER immobile fraction of mGluR5-GFP as determined by t test, $p > 0.5$. *N.A.*, not applicable, in this case because the immobile fraction is above 50% and the kinetics do not fit a diffusional profile. $n = 10$. *E,* proposed model of mGluR5 trafficking: current data indicate that >90% of mGluR5 traffics to the *trans*-Golgi network. Subsequently, ~15–60% (29, 30, 71, 74, 76, 77) of mGluR5 traffics to the PM where it appears to undergo a cycle of constitutive endocytosis and recycling (58). Remaining mGluR5 is retrogradely trafficked back to the ER where it can undergo lateral diffusion to reach the INM. INM receptors are held in place via interactions with the chromatin. *NPC,* nuclear pore complex.

C-terminal tail, one of which is within the INM localization sequence defined here. This sequence also completely overlaps one of two predicted calmodulin-binding sites suggesting that this region of the C terminus undergoes complex regulation. Indeed, several kinase structural motifs are contained within this sequence, including motifs for PKA, casein kinase II, PKC, and CaMKII (69). Conceivably, phosphorylation might influence binding by calmodulin or Norbin akin to the described role of sequences immediately adjacent (889–917), which encompass a PKC phosphorylation site (58). Roche and coworkers (70) have shown that binding of calmodulin within this domain promotes the interaction of the receptor on the plasma membrane. PKC phosphorylation at Ser-901 leads to the loss of calmodulin and the binding of Siah-1A, which promotes internalization (58). Conceivably, phosphorylation-dependent calmodulin binding prevents Norbin from trafficking mGluR5 to the cell surface. Alternatively, these sequences may serve as a binding site for an unknown protein(s) that helps re-distribute mGluR5 to the INM; deletion of 852–876 prevented this interaction (Fig. 4, *A* and *B*). Although these observations need to be supported with further investigation, it is clear that the sequence defined lies within a domain already notable for its complex regulation.

In summary, amino acids 852–876 of the rat mGluR5 C terminus are necessary and sufficient for the INM localization of the receptor. Given that no classic NLS sequences are present in this domain or the entire C terminus, lateral diffusion from the ONM to the INM seems a likely model to account for the pres-

ence of mGluR5 on the INM. Retention on the INM via interactions with the chromatin would maintain the receptor in this location (Fig. 13*E*). Given the presence of many putative phosphorylation motifs within the INM localization sequence defined here, we would predict that complex protein interactions play a role in shaping mGluR5's final destination.

Materials and Methods

Cell Culture—Human embryonic kidney cells (HEK293) were maintained in Dulbecco's modified Eagle's medium supplemented with 10% fetal bovine serum and transiently transfected using standard transfection techniques as described (30). Primary striatal neuronal cultures using neonatal 1-day-old rat pups were prepared and maintained as described (31). Stable cell lines were generated using standard transfection techniques followed by repetitive rounds of limiting dilution. For immunocytochemistry and Ca^{2+}-imaging experiments, HEK293 cells were plated on glass coverslips or 35-mm glass bottom culture dishes coated with 0.2 mg/ml poly-D-lysine and incubated at 37 °C and 5% CO_2.

Plasmids—All chimeric DNA constructs were generated using standard polymerase chain reaction (PCR) amplification methods with appropriate primers, and plasmids were confirmed by sequencing. N-terminal HA-tagged mGluR5a clone was generated previously (30). The $GABA_{B2}$ clone (30) was modified by the addition of an HA tag after the signal peptide. All other constructs were generated from either the HA-tagged mGluR5 or $GABA_{B2}$ construct. For all deletion constructs, the indicated amino acids are the first and the last amino acids of the regions deleted from the rat mGluR5 (Δ852–876 and Δ877–896) (NM_017012). $N_{mG5}C_{GB2}$ and $N_{GB2}C_{mG5}$ chimeric constructs were generated by adding cytoplasmic C-terminal amino acids 741–940 from $GABA_{B2}$ (NM_031802) to the C-terminal end of mGluR5 just 3′ to the last transmembrane domain (ending at amino acid 826) and vice versa. Additional clones were constructed such that increasing lengths of the mGluR5 C-terminal tail were added in front of the $GABA_{B2}$ C-terminal amino acids such that constructs $N_{mG5\_854}C_{GB2}$, $N_{mG5\_896}C_{GB2}$, and $N_{mG5\_966}C_{GB2}$ were created. The number indicates the last mGluR5 amino acid of the construct. Given the size constraints associated with the peripheral channel between the nuclear pore complex and the pore membrane (20), additional lengths of mGluR5 C terminus would have been confounding. Therefore, we inverted the paradigm and put additional pieces of the mGluR5 C terminus on the end of the $GABA_{B2}$ C-terminal tail. These included constructs $N_{GB2}C_{mG5\_827–966}$, $N_{GB2}C_{mG5\_967–1036}$, $N_{GB2}C_{mG5\_967–1106}$, and $N_{GB2}C_{mG5\_1107–1171}$. The $mGluR5_{\Delta KRR}$ construct was generated by mutating amino acids 866–868 (lysine, arginine, and arginine) to glutamine. The C-terminal truncated construct was created by adding a Kozak sequence and AUG (GCCGCCACCAUGG) in-frame with the HA motif and then the mGluR5 sequence from amino acids 827–966 followed by a stop codon. For the mGluR5 clone containing a BBS, the HA epitope was replaced with the BBS amino acids WRYYESSLEPYPD (52). For the dendra-labeled mGluR5 clone, the N-terminal HA epitope was removed and replaced by the dendra sequence in-frame with the full-length mGluR5 coding sequence. All the constructs described above were in pcDNA3 expression vector. IP_3 sponge constructs were constructed (47) and generously provided by Dr. Michael H. Nathanson, Yale University, New Haven, CT.

Immunocytochemistry—Cells were fixed, blocked, and incubated with antibody as described (31). For experiments in which cells were not permeabilized, they were blocked with 3% normal goat serum, incubated with the primary antibody at room temperature, fixed with 4% paraformaldehyde, reblocked, and labeled with secondary antibody. Primary antibodies included rabbit polyclonal anti-HA.11 (1:250, Covance, Princeton, NJ) and monoclonal anti-lamin B_2 (1:200, Zymed Laboratories Inc.). Secondary antibodies included goat anti-rabbit and goat anti-mouse Cy3 (both 1:300, Jackson ImmunoResearch, West Grove, PA), goat anti-rabbit Alexa 488 (1:500, Molecular Probes, Eugene, OR), goat anti-mouse Alexa 488 (1:300, Molecular Probes).

Subcellular Fractionation—HEK293 cells were grown to near confluency, washed twice with phosphate-buffered saline (PBS), incubated with 5 mM *N*-ethylmaleimide (Sigma) for 10 min, and harvested by scraping followed by centrifugation. Whole cell control fractions were taken after scraping. Homogenization and preparation of nuclear and membrane fractions were done as described (30). Nuclei were further purified using 25–35% (v/v) iodixanol (Accurate Chemical and Scientific Corporation, Westbury, NY) gradient as described in the manufacturer's instructions. Aliquots from each fraction were used for gel electrophoresis (34).

Western Blotting Analysis—Proteins obtained from subcellular fractionation were resuspended in lysis buffer (150 mM NaCl, 1 mM EDTA, 0.1% SDS, 1% Nonidet P-40, 0.5% sodium deoxycholate, 50 mM Tris-HCl, pH 7.5, and protease inhibitors Complete Tablets; Roche Applied Sciences). Protein concentrations of each fraction were determined using the Bradford assay (Bio-Rad). Lysates were subjected to SDS-PAGE, blotted as described (31), and probed with rabbit polyclonal anti-HA.11 (1:1000, Covance), monoclonal anti-lamin B_2 (1:2000, Zymed Laboratories Inc.), or polyclonal anti-pan-cadherin (1:2000, Cell Signaling Technology, Inc., Beverly, MA). Horseradish peroxidase-conjugated goat anti-rabbit IgG (1:5000, Cell Signaling Technology) or anti-mouse IgG (1:5000, Sigma) was used in conjunction with enhanced chemiluminescence (Amersham Biosciences) to detect the signal. Densitometric analyses were performed using the ChemiDoc™ XRS+ system (Bio-Rad) together with associated Image Lab™ software.

Deglycosylation—Deglycosylation of samples with Endo H (New England Biolabs, Ipswich, MA) or PNGase F (New England Biolabs) was performed as described (72). The mGluR5 HEK stable cell line was grown to near confluency, washed twice with phosphate-buffered saline (PBS), and harvested by scraping followed by centrifugation. Cells were homogenized, and nuclei and plasma membranes were prepared as described (30). The resultant nuclei and plasma membrane pellets were resuspended in buffer containing 75 mM Tris, 12.5 mM $MgCl_2$, 1 mM EDTA, pH 7.4, and protease inhibitors (Complete Tablets; Roche Applied Science). Aliquots (50 μg of protein) from each fraction were subjected to Endo H or PNGase F treatment. Samples were denatured in denaturing buffer (0.5% SDS and 1%

β-mercaptoethanol) at 55 °C for 10 min. The denatured samples were then subjected to digestion with 2500 units of Endo H in a 60-μl reaction mixture containing 50 mM sodium citrate, pH 5.5, 0.5% SDS, and 1% β-mercaptoethanol or with 2500 units of PNGase F in a 60-μl reaction mixture containing 50 mM sodium phosphate, pH 7.5, 0.5% SDS, 1% Nonidet P-40, and 1% β-mercaptoethanol for 4 h at 37 °C. The reactions were stopped by adding 0.2 volume of 5× sample buffer. The treated samples were analyzed by SDS-8.5% PAGE under reducing conditions.

Calcium Imaging—For whole cell measurements, transfected HEK293 cells were washed with serum-free medium, incubated with Oregon Green 488 BAPTA 1-AM (Molecular Probes), and imaged as described (34). To measure Ca^{2+} changes in individual nuclei, nuclei from HEK293 cells were prepared and processed as described (30). Extra- and intracellular buffers used in whole cell and nuclear Ca^{2+} imaging experiments were as described (31). Drugs ((*RS*)-3,5-dihydroxyphenylglycine (DHPG), Tocris Cookson Inc., Ellisville, MO; Quis, Tocris Cookson, Inc.; 2-amino-2-(3-*cis*- and *trans*-carboxycyclobutyl)-3-(9*H*-thioxanthen-9-yl)propionic acid (LY393053), Lilly; and 2-methyl-6-(phenylethynyl) pyridine (MPEP), Tocris Cookson Inc.) at ×100 concentration were added to the side of the dish and allowed to diffuse at room temperature.

Confocal Microscopy and Data Analysis—Ca^{2+} measurements and imaging of immunostained samples were done by using laser scanning confocal microscope Fluoview 500 (Olympus, Center Valley, PA) with an Olympus LUMPlanFl/lR ×20/0.50w, ×40/0.80w, or ×60/0.90w objective as described previously (30, 31). Images were analyzed with MetaMorph (version 5.0.7; Molecular Devices) Professional Image Analysis software. Images of HA-positive cells were taken such that the focal plane was centered on the NM demarcated by lamin B_2 staining. Images with saturated signals were excluded to avoid analysis of overexpressing cells. Immunostained samples were quantitated in a blind fashion such that regions from the plasma membrane and nuclear membrane were selected by using transmitted light images and lamin B_2 images, respectively, and the ratio of nuclear membrane to the plasma membrane was compared between different constructs. Line scan analysis was performed by randomly drawing a horizontal line near the center of the nucleus followed by a vertical line perpendicular to the first (73). Fluorescence intensity was quantified along both lines using MetaMorph software. For clarity, only the horizontal line is included in panel images. Background fluorescence was measured in an untransfected cell within the field and subtracted from the NM, PM, or ER fluorescence measurements. For each image, the NM pixel intensity was divided by ER or PM pixel intensity, and values from multiple cells were averaged to compute the NM/ER or NM/PM intensity ratio for each construct. The data shown represent the average of >15 cells per construct.

FRAP—FRAP experiments (74) were performed on a confocal laser scanning microscope Olympus FluoView™ FV1000 (Olympus, Melville, NY) equipped with objective UPLSAPO 60 × O NA:1.35 (Olympus). HEK cells transiently transfected with green fluorescent protein-tagged LBR or mGluR5 were maintained at 37 °C in an atmosphere containing 5% CO_2. Proteins were photobleached by a 10% 405-nm laser line, SIM Tornado (Olympus) for 100–300 ms. Images in the green channel were acquired using a 1–5% 488-nm laser and detection at 500–540 nm before and after photobleaching. The scanning laser intensity did not significantly photobleach the specimen over the time course of the experiment. To correct for photobleaching, a similar region of interest in a non-bleached area located in the same field of view was selected, and the time-dependent decrease in fluorescence was used to correct the recovery curves. The corrected fluorescence recovery was analyzed using MetaMorph image analysis software and curve fitted using the one-phase association exponential equation from GraphPad Prism (San Diego). The average fluorescence before photobleaching was counted as 100%. The mobile fraction was defined as the fluorescence intensity after full recovery divided by the fluorescence intensity before photobleaching. Diffusion coefficients (*D*) were calculated from confocal FRAP data using the half-time of recovery ($\tau_{1/2}$) and the simplified Equation 1,

$$D = 0.25\frac{r_n^2}{\tau_{1/2}} \qquad \text{(Eq. 1)}$$

which holds when $r_e = r_n$, *i.e.* when the effective postbleach radius (r_e) equals r_n (the nominal or user-defined bleaching spot radius) as described (75).

Photoconversion of Dendra-mGluR5—An Olympus FluoView™ FV1000 with objective UPLSAPO ×60 Oil NA:1.35 (Olympus) was used. Dendra-mGluR5-transfected HEK cells were plated in imaging chambers using phenol-red free DMEM 10% (v/v) fetal bovine serum, 2 mM glutamine, and 25 mM HEPES, pH 7.4, at 37 °C (42). A small ROI on the ER or nuclear membrane was photoactivated by a 5–15% 405-nm laser line, SIM Tornado (Olympus), for 200–500 ms. Green channel images before photoactivation were obtained using the 488-nm laser (2%) and detection at 500–540 nm. Red channel images before and after photoconversion were obtained using the 543-nm laser (50%) and detection at 560–670 nm. Movement of the photoactivated red fluorescent protein was observed by measuring the fluorescence intensities in the ROI using MetaMorph image analysis software.

Chromatin Immunoprecipitation—Chromatin immunoprecipitation experiments were done as described previously (36) starting with ~5×10^6 cells transfected with the indicated constructs. Lysates were first cross-linked and then immunoprecipitated with 2–4 μg of anti-HA or nonspecific IgG (Millipore Corp., Billerica, MA) at 4 °C overnight. Immune complexes were collected, washed, eluted, and reverse cross-linked. Eluted DNA was purified and used as a template for PCR with primers designed to detect human repetitive Sx/Sg and Y subfamilies of Alu (55): forward primer, GGCGCGGTGGCTCACGCC, and reverse primer, GAGACGGAGTCTCGCTCT.

Author Contributions—I. S., Y. I. J., and K. L. O. designed the study and wrote the paper. I. S. performed and analyzed the experiments shown in Figs. 1–8. Y. I. J. performed and analyzed the experiments shown in Figs. 3, 4, and 9–11. V. K. made the mGluR5 chimeric constructs. S. K. H. made many of the mGluR5-deleted constructs, prepared striatal cultures, and performed figure editing. All authors reviewed the results and approved the final version of the manuscript.

Acknowledgments—We thank Dr. M. Nathanson (Yale University) for IP_3 sponge constructs. Microscopes and software were provided in part through the use of Washington University Center for Cellular Imaging (WUCCI) supported by Washington University School of Medicine, The Children's Discovery Institute of Washington University and St. Louis Children's Hospital (CDI-CORE-2015-505), and the NINDS, National Institutes of Health (NS086741).

References

1. Jong, Y. J., Sergin, I., Purgert, C. A., and O'Malley, K. L. (2014) Location-dependent signaling of the group 1 metabotropic glutamate receptor mGlu5. *Mol. Pharmacol.* **86,** 774–785
2. Branco, A. F., and Allen, B. G. (2015) G protein-coupled receptor signaling in cardiac nuclear membranes. *J. Cardiovasc. Pharmacol.* **65,** 101–109
3. Campden, R., Audet, N., and Hébert, T. E. (2015) Nuclear G protein signaling: new tricks for old dogs. *J. Cardiovasc. Pharmacol.* **65,** 110–122
4. Irannejad, R., and von Zastrow, M. (2014) GPCR signaling along the endocytic pathway. *Curr. Opin. Cell Biol.* **27,** 109–116
5. Calebiro, D., Godbole, A., Lyga, S., and Lohse, M. J. (2015) Trafficking and function of GPCRs in the endosomal compartment. *Methods Mol. Biol.* **1234,** 197–211
6. Bénard, G., Massa, F., Puente, N., Lourenço, J., Bellocchio, L., Soria-Gómez, E., Matias, I., Delamarre, A., Metna-Laurent, M., Cannich, A., Hebert-Chatelain, E., Mulle, C., Ortega-Gutiérrez, S., Martín-Fontecha, M., Klugmann, M., *et al.* (2012) Mitochondrial CB(1) receptors regulate neuronal energy metabolism. *Nat. Neurosci.* **15,** 558–564
7. Meads, M. B., and Medveczky, P. G. (2004) Kaposi's sarcoma-associated herpesvirus-encoded viral interleukin-6 is secreted and modified differently than human interleukin-6: evidence for a unique autocrine signaling mechanism. *J. Biol. Chem.* **279,** 51793–51803
8. Rozenfeld, R., and Devi, L. A. (2008) Regulation of CB1 cannabinoid receptor trafficking by the adaptor protein AP-3. *FASEB J.* **22,** 2311–2322
9. Oksche, A., Boese, G., Horstmeyer, A., Furkert, J., Beyermann, M., Bienert, M., and Rosenthal, W. (2000) Late endosomal/lysosomal targeting and lack of recycling of the ligand-occupied endothelin B receptor. *Mol. Pharmacol.* **57,** 1104–1113
10. Calebiro, D., Nikolaev, V. O., Persani, L., and Lohse, M. J. (2010) Signaling by internalized G-protein-coupled receptors. *Trends Pharmacol. Sci.* **31,** 221–228
11. Gobeil, F., Fortier, A., Zhu, T., Bossolasco, M., Leduc, M., Grandbois, M., Heveker, N., Bkaily, G., Chemtob, S., and Barbaz, D. (2006) G-protein-coupled receptors signalling at the cell nucleus: an emerging paradigm. *Can. J. Physiol. Pharmacol.* **84,** 287–297
12. Tadevosyan, A., Vaniotis, G., Allen, B. G., Hébert, T. E., and Nattel, S. (2012) G protein-coupled receptor signalling in the cardiac nuclear membrane: evidence and possible roles in physiological and pathophysiological function. *J. Physiol.* **590,** 1313–1330
13. Lee, D. K., Lança, A. J., Cheng, R., Nguyen, T., Ji, X. D., Gobeil, F., Jr, Chemtob, S., George, S. R., and O'Dowd, B. F. (2004) Agonist-independent nuclear localization of the Apelin, angiotensin AT1, and bradykinin B2 receptors. *J. Biol. Chem.* **279,** 7901–7908
14. Morinelli, T. A., Raymond, J. R., Baldys, A., Yang, Q., Lee, M. H., Luttrell, L., and Ullian, M. E. (2007) Identification of a putative nuclear localization sequence within ANG II AT(1A) receptor associated with nuclear activation. *Am. J. Physiol. Cell Physiol.* **292,** C1398–C1408
15. Wright, C. D., Wu, S. C., Dahl, E. F., Sazama, A. J., and O'Connell, T. D. (2012) Nuclear localization drives α1-adrenergic receptor oligomerization and signaling in cardiac myocytes. *Cell. Signal.* **24,** 794–802
16. Joyal, J. S., Nim, S., Zhu, T., Sitaras, N., Rivera, J. C., Shao, Z., Sapieha, P., Hamel, D., Sanchez, M., Zaniolo, K., St-Louis, M., Ouellette, J., Montoya-Zavala, M., Zabeida, A., Picard, E., *et al.* (2014) Subcellular localization of coagulation factor II receptor-like 1 in neurons governs angiogenesis. *Nat. Med.* **20,** 1165–1173
17. Boivin, B., Vaniotis, G., Allen, B. G., and Hébert, T. E. (2008) G protein-coupled receptors in and on the cell nucleus: a new signaling paradigm? *J. Recept. Signal. Transduct. Res.* **28,** 15–28
18. Barlow, C. A., Laishram, R. S., and Anderson, R. A. (2010) Nuclear phosphoinositides: a signaling enigma wrapped in a compartmental conundrum. *Trends Cell Biol.* **20,** 25–35
19. Purgert, C. A., Izumi, Y., Jong, Y. J., Kumar, V., Zorumski, C. F., and O'Malley, K. L. (2014) Intracellular mGluR5 can mediate synaptic plasticity in the hippocampus. *J. Neurosci.* **34,** 4589–4598
20. Zuleger, N., Kerr, A. R., and Schirmer, E. C. (2012) Many mechanisms, one entrance: membrane protein translocation into the nucleus. *Cell. Mol. Life Sci.* **69,** 2205–2216
21. Katta, S. S., Smoyer, C. J., and Jaspersen, S. L. (2014) Destination: inner nuclear membrane. *Trends Cell Biol.* **24,** 221–229
22. Lusk, C. P., Blobel, G., and King, M. C. (2007) Highway to the inner nuclear membrane: rules for the road. *Nat. Rev. Mol. Cell Biol.* **8,** 414–420
23. Hinshaw, J. E., Carragher, B. O., and Milligan, R. A. (1992) Architecture and design of the nuclear pore complex. *Cell* **69,** 1133–1141
24. Zuleger, N., Korfali, N., and Schirmer, E. C. (2008) Inner nuclear membrane protein transport is mediated by multiple mechanisms. *Biochem. Soc. Trans.* **36,** 1373–1377
25. Reichelt, R., Holzenburg, A., Buhle, E. L., Jr, Jarnik, M., Engel, A., and Aebi, U. (1990) Correlation between structure and mass distribution of the nuclear pore complex and of distinct pore complex components. *J. Cell Biol.* **110,** 883–894
26. Holzenburg, A., Wilson, F. H., Finbow, M. E., and Ford, R. C. (1992) Structural investigations of membrane proteins: the versatility of electron microscopy. *Biochem. Soc. Trans.* **20,** 591–597
27. Soullam, B., and Worman, H. J. (1995) Signals and structural features involved in integral membrane protein targeting to the inner nuclear membrane. *J. Cell Biol.* **130,** 15–27
28. Zuleger, N., Kelly, D. A., Richardson, A. C., Kerr, A. R., Goldberg, M. W., Goryachev, A. B., and Schirmer, E. C. (2011) System analysis shows distinct mechanisms and common principles of nuclear envelope protein dynamics. *J. Cell Biol.* **193,** 109–123
29. Hubert, G. W., Paquet, M., and Smith, Y. (2001) Differential subcellular localization of mGluR1a and mGluR5 in the rat and monkey substantia nigra. *J. Neurosci.* **21,** 1838–1847
30. O'Malley, K. L., Jong, Y. J., Gonchar, Y., Burkhalter, A., and Romano, C. (2003) Activation of metabotropic glutamate receptor mGlu5 on nuclear membranes mediates intranuclear Ca^{2+} changes in heterologous cell types and neurons. *J. Biol. Chem.* **278,** 28210–28219
31. Jong, Y. J., Kumar, V., Kingston, A. E., Romano, C., and O'Malley, K. L. (2005) Functional metabotropic glutamate receptors on nuclei from brain and primary cultured striatal neurons. Role of transporters in delivering ligand. *J. Biol. Chem.* **280,** 30469–30480
32. Hermans, E., and Challiss, R. A. (2001) Structural, signalling and regulatory properties of the group I metabotropic glutamate receptors: prototypic family C G-protein-coupled receptors. *Biochem. J.* **359,** 465–484
33. Vincent, K., Cornea, V. M., Jong, Y. J., Laferrière, A., Kumar, N., Mickeviciute, A., Fung, J. S., Bandegi, P., Ribeiro-da-Silva, A., O'Malley, K. L., Coderre T. J. (2016) Intracellular mGluR5 plays a critical role in neuropathic pain. *Nat. Commun.* **7,** 10604
34. Kumar, V., Jong, Y. J., and O'Malley, K. L. (2008) Activated nuclear metabotropic glutamate receptor mGlu5 couples to nuclear Gq/11 proteins to generate inositol 1,4,5-trisphosphate-mediated nuclear Ca^{2+} release. *J. Biol. Chem.* **283,** 14072–14083
35. Kumar, V., Fahey, P. G., Jong, Y. J., Ramanan, N., and O'Malley, K. L. (2012) Activation of intracellular metabotropic glutamate receptor 5 in striatal neurons leads to up-regulation of genes associated with sustained synaptic transmission including Arc/Arg3.1 protein. *J. Biol. Chem.* **287,** 5412–5425
36. Jong, Y. J., Kumar, V., and O'Malley, K. L. (2009) Intracellular metabotropic glutamate receptor 5 (mGluR5) activates signaling cascades distinct from cell surface counterparts. *J. Biol. Chem.* **284,** 35827–35838
37. Walther, C., and Ferguson, S. S. (2013) Arrestins: role in the desensitization, sequestration, and vesicular trafficking of G protein-coupled receptors. *Prog. Mol. Biol. Transl. Sci.* **118,** 93–113

38. Magalhaes, A. C., Dunn, H., and Ferguson, S. S. (2012) Regulation of GPCR activity, trafficking and localization by GPCR-interacting proteins. *Br. J. Pharmacol.* **165,** 1717–1736
39. Dunn, H. A., and Ferguson, S. S. (2015) PDZ protein regulation of GPCR trafficking and signaling pathways. *Mol. Pharmacol.* **88,** 624–639
40. Dores, M. R., and Trejo, J. (2014) Atypical regulation of G protein-coupled receptor intracellular trafficking by ubiquitination. *Curr. Opin. Cell Biol.* **27,** 44–50
41. Shirvani, H., Gätà, G., and Marullo, S. (2012) Regulated GPCR trafficking to the plasma membrane: general issues and the CCR5 chemokine receptor example. *Subcell. Biochem.* **63,** 97–111
42. Margeta-Mitrovic, M., Jan, Y. N., and Jan, L. Y. (2000) A trafficking checkpoint controls GABA(B) receptor heterodimerization. *Neuron* **27,** 97–106
43. White, J. H., Wise, A., Main, M. J., Green, A., Fraser, N. J., Disney, G. H., Barnes, A. A., Emson, P., Foord, S. M., and Marshall, F. H. (1998) Heterodimerization is required for the formation of a functional GABA(B) receptor. *Nature* **396,** 679–682
44. Lester, H. A., Miwa, J. M., and Srinivasan, R. (2012) Psychiatric drugs bind to classical targets within early exocytotic pathways: therapeutic effects. *Biol. Psychiatry* **72,** 907–915
45. Francesconi, A., and Duvoisin, R. M. (1998) Role of the second and third intracellular loops of metabotropic glutamate receptors in mediating dual signal transduction activation. *J. Biol. Chem.* **273,** 5615–5624
46. Kniazeff, J., Bessis, A. S., Maurel, D., Ansanay, H., Prézeau, L., and Pin, J. P. (2004) Closed state of both binding domains of homodimeric mGlu receptors is required for full activity. *Nat. Struct. Mol. Biol.* **11,** 706–713
47. Gomes, D. A., Rodrigues, M. A., Leite, M. F., Gomez, M. V., Varnai, P., Balla, T., Bennett, A. M., and Nathanson, M. H. (2008) c-Met must translocate to the nucleus to initiate calcium signals. *J. Biol. Chem.* **283,** 4344–4351
48. Gerasimenko, O. V., Gerasimenko, J. V., Tepikin, A. V., and Petersen, O. H. (1995) ATP-dependent accumulation and inositol trisphosphate- or cyclic ADP-ribose-mediated release of Ca^{2+} from the nuclear envelope. *Cell* **80,** 439–444
49. Bhave, G., Nadin, B. M., Brasier, D. J., Glauner, K. S., Shah, R. D., Heinemann, S. F., Karim, F., and Gereau, R. W., 4th (2003) Membrane topology of a metabotropic glutamate receptor. *J. Biol. Chem.* **278,** 30294–30301
50. Poon, I. K., and Jans, D. A. (2005) Regulation of nuclear transport: central role in development and transformation? *Traffic* **6,** 173–186
51. Goldfarb, D. S., Corbett, A. H., Mason, D. A., Harreman, M. T., and Adam, S. A. (2004) Importin α: a multipurpose nuclear-transport receptor. *Trends Cell Biol.* **14,** 505–514
52. Sekine-Aizawa, Y., and Huganir, R. L. (2004) Imaging of receptor trafficking by using α-bungarotoxin-binding-site-tagged receptors. *Proc. Natl. Acad. Sci. U.S.A.* **101,** 17114–17119
53. Trivedi, R. R., and Bhattacharyya, S. (2012) Constitutive internalization and recycling of metabotropic glutamate receptor 5 (mGluR5). *Biochem. Biophys. Res. Commun.* **427,** 185–190
54. Ulbert, S., Platani, M., Boue, S., and Mattaj, I. W. (2006) Direct membrane protein-DNA interactions required early in nuclear envelope assembly. *J. Cell Biol.* **173,** 469–476
55. Batzer, M. A., and Deininger, P. L. (2002) Alu repeats and human genomic diversity. *Nat. Rev. Genet.* **3,** 370–379
56. Marfori, M., Mynott, A., Ellis, J. J., Mehdi, A. M., Saunders, N. F., Curmi, P. M., Forwood, J. K., Bodén, M., and Kobe, B. (2011) Molecular basis for specificity of nuclear import and prediction of nuclear localization. *Biochim. Biophys. Acta* **1813,** 1562–1577
57. Fourgeaud, L., Bessis, A. S., Rossignol, F., Pin, J. P., Olivo-Marin, J. C., and Hémar, A. (2003) The metabotropic glutamate receptor mGluR5 is endocytosed by a clathrin-independent pathway. *J. Biol. Chem.* **278,** 12222–12230
58. Francesconi, A., Kumari, R., and Zukin, R. S. (2009) Regulation of group I metabotropic glutamate receptor trafficking and signaling by the caveolar/lipid raft pathway. *J. Neurosci.* **29,** 3590–3602
59. Benyair, R., Ogen-Shtern, N., and Lederkremer, G. Z. (2015) Glycan regulation of ER-associated degradation through compartmentalization. *Semin. Cell Dev. Biol.* **41,** 99–109
60. Abe, T., Sugihara, H., Nawa, H., Shigemoto, R., Mizuno, N., and Nakanishi, S. (1992) Molecular characterization of a novel metabotropic glutamate receptor mGluR5 coupled to inositol phosphate/Ca^{2+} signal transduction. *J. Biol. Chem.* **267,** 13361–13368
61. Gruenbaum, Y., Margalit, A., Goldman, R. D., Shumaker, D. K., and Wilson, K. L. (2005) The nuclear lamina comes of age. *Nat. Rev. Mol. Cell Biol.* **6,** 21–31
62. Schirmer, E. C., and Foisner, R. (2007) Proteins that associate with lamins: many faces, many functions. *Exp. Cell Res.* **313,** 2167–2179
63. Holmer, L., and Worman, H. J. (2001) Inner nuclear membrane proteins: functions and targeting. *Cell. Mol. Life Sci.* **58,** 1741–1747
64. Prokocimer, M., Davidovich, M., Nissim-Rafinia, M., Wiesel-Motiuk, N., Bar, D. Z., Barkan, R., Meshorer, E., and Gruenbaum, Y. (2009) Nuclear lamins: key regulators of nuclear structure and activities. *J. Cell Mol. Med.* **13,** 1059–1085
65. Olins, A. L., Rhodes, G., Welch, D. B., Zwerger, M., and Olins, D. E. (2010) lamin B receptor: multi-tasking at the nuclear envelope. *Nucleus* **1,** 53–70
66. Ye, Q., and Worman, H. J. (1994) Primary structure analysis and lamin B and DNA binding of human LBR, an integral protein of the nuclear envelope inner membrane. *J. Biol. Chem.* **269,** 11306–11311
67. Ribeiro, F. M., Paquet, M., Cregan, S. P., and Ferguson, S. S. (2010) Group I metabotropic glutamate receptor signalling and its implication in neurological disease. *CNS Neurol. Disord. Drug Targets* **9,** 574–595
68. Wang, H., Westin, L., Nong, Y., Birnbaum, S., Bendor, J., Brismar, H., Nestler, E., Aperia, A., Flajolet, M., and Greengard, P. (2009) Norbin is an endogenous regulator of metabotropic glutamate receptor 5 signaling. *Science* **326,** 1554–1557
69. Mao, L. M., Liu, X. Y., Zhang, G. C., Chu, X. P., Fibuch, E. E., Wang, L. S., Liu, Z., and Wang, J. Q. (2008) Phosphorylation of group I metabotropic glutamate receptors (mGluR1/5) in vitro and in vivo. *Neuropharmacology* **55,** 403–408
70. Ko, S. J., Isozaki, K., Kim, I., Lee, J. H., Cho, H. J., Sohn, S. Y., Oh, S. R., Park, S., Kim, D. G., Kim, C. H., and Roche, K. W. (2012) PKC phosphorylation regulates mGluR5 trafficking by enhancing binding of Siah-1A. *J. Neurosci.* **32,** 16391–16401
71. Petralia, R. S., Wang, Y. X., Singh, S., Wu, C., Shi, L., Wei, J., and Wenthold, R. J. (1997) A monoclonal antibody shows discrete cellular and subcellular localizations of mGluR1 α metabotropic glutamate receptors. *J. Chem. Neuroanat.* **13,** 77–93
72. Hurt, C. M., Ho, V. K., and Angelotti, T. (2013) Systematic and quantitative analysis of G protein-coupled receptor trafficking motifs. *Methods Enzymol.* **521,** 171–187
73. Goodchild, R. E., Buchwalter, A. L., Naismith, T. V., Holbrook, K., Billion, K., Dauer, W. T., Liang, C. C., Dear, M. L., and Hanson, P. I. (2015) Access of torsinA to the inner nuclear membrane is activity dependent and regulated in the endoplasmic reticulum. *J. Cell Sci.* **128,** 2854–2865
74. Snapp, E. L., Altan, N., and Lippincott-Schwartz, J. (2003) Measuring protein mobility by photobleaching GFP chimeras in living cells. *Curr. Protoc. Cell Biol.* Chapter 21, Unit 21.21
75. Kang, M., Day, C. A., Kenworthy, A. K., and DiBenedetto, E. (2012) Simplified equation to extract diffusion coefficients from confocal FRAP data. *Traffic* **13,** 1589–1600
76. Luján, R., Roberts, J. D., Shigemoto, R., Ohishi, H., and Somogyi, P. (1997) Differential plasma membrane distribution of metabotropic glutamate receptors mGluR1 α, mGluR2 and mGluR5, relative to neurotransmitter release sites. *J. Chem. Neuroanat.* **13,** 219–241
77. López-Bendito, G., Shigemoto, R., Fairén, A., and Luján, R. (2002) Differential distribution of group I metabotropic glutamate receptors during rat cortical development. *Cereb. Cortex.* **12,** 625–638

Sequences within the C Terminus of the Metabotropic Glutamate Receptor 5 (mGluR5) Are Responsible for Inner Nuclear Membrane Localization

Ismail Sergin, Yuh-Jiin I. Jong, Steven K. Harmon, Vikas Kumar and Karen L. O'Malley

J. Biol. Chem. 2017, 292:3637-3655.
doi: 10.1074/jbc.M116.757724 originally published online January 17, 2017
